Citation: Sequero, C., Della Porta, G., Bádenas, B., Aurell, M., 2021. Carbon and oxygen stable isotope record of upper Kimmeridgian shallow-marine ramp carbonates (Iberian Basin, NE Spain): the imprint of different burial and tectonic histories. Geologica Acta,19.14, 1-23.
DOI: 10.1344/GeologicaActa2021.19.14

Carbon and oxygen stable isotope record of upper Kimmeridgian shallow-marine ramp carbonates (Iberian Basin, NE Spain): the imprint of different burial and tectonic histories

Cristina Sequero[1] **Giovanna Della Porta**[2] **Beatriz Bádenas**[1] **Marcos Aurell**[1]

[1]**Departamento de Ciencias de la Tierra-IUCA, Universidad de Zaragoza**
50009, Zaragoza, Spain. Sequero E-mail: cristinasq92@gmail.com;
Bádenas E-mail: bbadenas@unizar.es; Aurell E-mail: maurell@unizar.es

[2]**Dipartimento di Scienze della Terra "Ardito Desio", Università degli Studi di Milano**
20133, Milano, Italy. E-mail: giovanna.dellaporta@unimi.it

ABSTRACT

Bulk carbon and oxygen stable isotopes of ancient shallow-marine carbonates can record the effects of multiple palaeoenvironmental factors, but also the imprint of several post-depositional processes, which may alter the original marine isotopic composition. In this study, carbon and oxygen stable isotope analyses were performed on bulk carbonate, bivalve calcitic-shell (*Trichites*) and calcite vein samples from two stratigraphic sections (Tosos and Fuendetodos, present-day distance 15km), representing proximal inner- and distal mid-ramp environments, respectively, of the uppermost Kimmeridgian ramp facies deposited in the northern Iberian Basin (NE Spain). These successions underwent different diagenetic pathways that altered the primary marine isotopic composition in each section in different ways. Different burial histories, tectonic uplift and a variable exposure to meteoric diagenesis from the end of the Kimmeridgian to the Cenozoic (following Alpine tectonic uplift) are reflected in the different alteration patterns of the carbon and oxygen stable isotope signatures. A significant deviation to lower values in both $\delta^{13}C$ and $\delta^{18}O$ is recorded in those carbonates mostly exposed to meteoric diagenesis (distal mid-ramp Fuendetodos section), because of post-depositional tectonic uplift (telogenesis). On the other hand, the deposits mainly affected by burial diagenesis (proximal inner-ramp Tosos section) only record low $\delta^{18}O$ with respect to expected values for pristine Kimmeridgian marine carbonates. The different burial and tectonic uplift histories of these deposits in each sector, due to their different tectonic evolution in this part of the basin, resulted in a variable degree of diagenetic resetting. However, in spite of the different diagenetic resetting reported of the carbon and oxygen stable isotope signatures in each section, these carbonates show similar cement types in terms of fabrics and cathodoluminescence properties. The diagenetic resetting reported for these carbonates prevents the use of the $\delta^{13}C$ and $\delta^{18}O$ records for addressing palaeoenvironmental interpretations, but instead highlights useful features regarding the variable diagenetic overprint of the studied shallow-marine carbonate successions concerning their specific post-depositional history.

KEYWORDS | **Carbonate ramp facies; Carbon and oxygen isotopes; Diagenetic resetting; Post-depositional history; Tectonic uplift.**

INTRODUCTION

Using the carbon and oxygen stable isotope composition of shallow-marine carbonates as proxies for palaeo-seawater, palaeoclimatic and palaeoceanographic reconstructions is generally challenging, due to several factors. i) Multiple local and global processes control the chemical variability and isotopic signature of shallow seawaters and DIC (Dissolved Inorganic Carbon), including: evaporation, local stagnation of marine waters, input of freshwater through rainfall and rivers, latitude, climate, and perturbations of the carbon cycle (Castro *et al.,* 2019; Colombié *et al.,* 2011; Immenhauser *et al.,* 2003; Patterson and Walter, 1994; Swart, 2015; Zuo *et al.,* 2018). ii) In bulk carbonate samples, different components record potential distinctive isotopic compositions due to the precipitation processes and the vital effect on carbon isotope fractionation (*e.g.* skeletal grains, coated grains, micrite matrix) (Anderson and Arthur, 1983; Hudson, 1977; Jenkyns and Clayton, 1986; McConnaughey, 1989a, b; Nelson and Smith, 1996; Schobben *et al.,* 2015). iii) Diagenetic processes, from early meteoric eogenesis due to subaerial exposure to burial mesogenesis and meteoric telogenesis, can alter the primary marine isotopic signature, thus complicating the use of these isotopic records as palaeoenvironmental proxies (Brand and Veizer, 1981; Coimbra *et al.,* 2014; Glumac and Walker, 1998; Huck *et al.,* 2017; Immenhauser *et al.,* 2002; Marshall, 1992; Moore, 1989; Oehlert and Swart, 2019).

The magnitude of the diagenetic alteration can be variable for specific carbonate grains, depending on the original mineralogy and its degree of stability, increasing from aragonite, high-Mg calcite to low-Mg calcite. On the other hand, the magnitude of the diagenetic alteration also depends on the microstructure of the grains and on the degree of the primary porosity and permeability of the sediment. Coarse-grained grain-supported fabrics, in the absence of mud between grains, can be more favourable for infiltration of diagenetic fluids, and may result in a higher degree of diagenetic alteration and resetting of stable isotope signatures (Al-Mojel *et al.,* 2018; Coimbra *et al.,* 2014; Huck *et al.,* 2017; Immenhauser *et al.,* 2002; Marshall, 1992; Vincent *et al.,* 2004). Different diagenetic processes and products result from the interaction between carbonate sediments and rocks with diagenetic fluids of a different nature (*e.g.* seawater, meteoric waters, high-temperature burial or hydrothermal fluids). Which processes take place and the way they affect more intensively the sediment depend on multiple factors, such as the mineralogy, porosity and permeability of the carbonates, chemistry and saturation of the diagenetic fluid, temperature or pressure conditions, and the burial and tectonic history, among others. Diagenetic processes can involve the dissolution and re-precipitation of variable mineralogies (*e.g.* neomorphism of aragonite into low-Mg calcite), the formation of more stable mineralogical phases (*e.g.* high-Mg calcite to low-Mg calcite) or dolomite replacement (Allan and Matthews, 1982; Al-Mojel *et al.,* 2018; Brand *et al.,* 2012; Carpenter and Lohmann, 1989, 1997; Coimbra *et al.,* 2014; Given and Lohmann, 1985; Jenkyns and Clayton, 1986; Joachimski, 1994; van der Kooij *et al.,* 2009; Moore, 1989; O'Neil, 1977; Sharp, 2007; Tucker, 1993). Therefore, diagenetic processes usually are associated with chemical, mineralogical and/or textural changes of carbonates. These must be taken into account when interpreting the carbon and oxygen isotope signature of bulk rocks and specific diagenetic phases (Brand and Veizer, 1980, 1981; Coimbra *et al.,* 2014; Colombié *et al.,* 2011; Huck *et al.,* 2017; Lavoie and Bourque, 1993).

Diagenesis of marine carbonates commonly implies a decrease in $\delta^{18}O$ values by the influence of ^{18}O-depleted meteoric waters and/or relatively high-temperature burial fluids (due to the temperature dependence of oxygen isotopic fractionation). The magnitude of such alteration depends on the degree of the fluid-rock interaction (Allan and Matthews, 1982; Al-Mojel *et al.,* 2018; Brand and Veizer, 1980; Coimbra *et al.,* 2014; Given and Lohmann, 1985; Grotzinger *et al.,* 2011; Hudson, 1977; van der Kooij *et al.,* 2009; Madden and Wilson, 2013; Plunkett, 1997). Post-depositional alteration also generally leads to a decrease in $\delta^{13}C$ values, which is normally attributed to the interaction with meteoric fluids enriched in organic ^{12}C by soil weathering during penecontemporaneous subaerial exposure or during uplift after burial (telogenesis) (Allan and Matthews, 1982; Bahamonde *et al.,* 2017; Derry, 2010; Huck *et al.,* 2017; Hudson, 1977; Immenhauser *et al.,*2002; Lavastre *et al.,* 2011; Lohmann, 1988; Moore, 2001; O'Neil, 1987; Patterson and Walter, 1994; Swart, 2015). In this sense, the degradation of buried organic matter or the presence of hydrocarbon and methane seeps can also act as source of ^{12}C during the post-depositional burial stages (Chung *et al.,* 1992; Peckmann and Thiel, 2004). In ancient shallow-marine carbonate rock successions, the effect of meteoric and/or burial diagenesis on the carbon and oxygen stable isotope record has been highlighted in several studies. These works report local negative $\delta^{13}C$ and $\delta^{18}O$ excursions in bulk carbonates with coarser fabrics related to meteoric dissolution and cementation, neomorphism and recrystallization during subaerial exposure (vadose and phreatic zone), or decreasing $\delta^{18}O$ values from burial cements (Al-Mojel *et al.,* 2018; Coimbra *et al.,* 2014; Huck *et al.,* 2017; Immenhauser *et al.,* 2003; Strasser, 2015). However, some authors propose that even in the presence of diagenetic alteration, carbon and oxygen stable isotope compositions can provide some valuable information about the palaeoenvironmental setting (Al-Mojel *et al.,* 2018; Bartolini *et al.,* 2003; Colombié *et al.,* 2011; Zuo *et al.,* 2018), even using the carbon stable isotope stratigraphy as

a correlation tool between widely spaced separated logs (Colombié *et al.,* 2011; Eltom *et al.,* 2018; Glumac and Walker, 1998; Grötsch *et al.,* 1998; Zuo *et al.,* 2018).

In this study, bulk carbon and oxygen stable isotope analyses were performed on samples from two stratigraphic sections of the Higueruelas Formation cropping out in the north-eastern area of the Iberian Chain (NE Spain). These successions represent the proximal and relatively distal areas of the uppermost Kimmeridgian (Upper Jurassic) carbonate ramp that developed in the north-central part of the Iberian Basin. These sections were selected to evaluate the influence of depositional facies and palaeoenvironmental conditions on the recorded stable carbon and oxygen isotope signatures. However, the obtained results show that post-depositional processes had a strong influence on the recorded isotopic compositions in each sector linked to their specific burial evolution and tectonic uplift history, mostly related to the Early Cretaceous and Cenozoic tectono-sedimentary evolution in this part of the Iberian Basin. The major objectives of this study are: i) to evaluate the diagenetic features and their influence on the carbon and oxygen stable isotope signatures of these shallow-marine carbonate ramp deposits in two selected sections affected by different post-depositional histories, and ii) to discuss the potential of possible primary signals from the stable isotope data with a local and/or regional significance.

GEOLOGICAL SETTING

The studied uppermost Kimmeridgian Higueruelas Formation (Fm.) represents inner- to mid-ramp deposits of a carbonate ramp that developed in the north-central part of the Iberian Basin (Aurell *et al.,* 2003, 2010) (Fig. 1A, B). At basin scale, these shallow-marine deposits grade eastwards into outer-ramp marlstone and lime mudstone of the Loriguilla Fm. (Aurell *et al.,* 2003, 2010) (Fig. 1C). The regional relative sea-level fall documented at the end of the Kimmeridgian, which was partly controlled by the rifting-related tectonic uplift of the Iberian Massif (Fig. 1A), resulted in a gradual shallowing-upward trend and the final subaerial exposure of the carbonate ramp in this part of the basin due to tectonic uplift (Aurell *et al.,* 2003; Bádenas and Aurell, 2001). The shallowing-upward trend at the end of the Kimmeridgian culminated with deposition of a mixed carbonate-siliciclastic unit overlying the Higueruelas Fm. (laterally equivalent to the Cedrillas Fm. recently defined in nearby areas by Aurell *et al.,* 2019) (Fig. 1C).

The Higueruelas Fm. is exposed in a set of W-E and NW-SE oriented anticlines located south of the city of Zaragoza (NE Spain) (Fig. 2A), which represent Cenozoic Alpine structures within the north-central Iberian Chain (Guimerà and Álvaro, 1990). In this area, the Higueruelas Fm. is 40 to 80m thick, and is characterized by packstone and grainstone with a wide variety of skeletal and non-skeletal grains (mainly peloids, ooids and oncoids), and local chaetetid-stromatoporoid-coral buildups (Aurell and Meléndez, 1986; Aurell *et al.,* 2012; Bádenas and Aurell, 2003; Ipas *et al.,* 2004; Sequero *et al.,* 2019, 2020). Detailed stratigraphic and sedimentological studies identified 9 correlatable metre- to decametre-thick high-frequency sequences in the Higueruelas Fm., which were tentatively interpreted as short-term (100kyr) eccentricity cycles (4th order cycles; Sequero *et al.,* 2019). In this study, the 4th order sequences 1 to 7 of two sedimentary sections, representing inner-ramp (Tosos section) and mid-ramp (Fuendetodos section) environments, have been investigated (Figs. 1B; 2A).

The tectonic uplift of the north-central Iberian Basin margin, leading to the subaerial exposure of the carbonate ramp at the end of the Kimmeridgian, was related to the Late Jurassic-Early Cretaceous rifting stage of the Iberian Basin (Fig. 3), followed by the subsequent post-rifting stage until the end of the Cretaceous (Aurell *et al.,* 2019; Cortés *et al.,* 1999). This resulted in the formation of several sub-basins controlled by extensional faults, which were inverted during the Cenozoic Alpine compression (Aurell *et al.,* 2019; Guimerà and Álvaro, 1990; Liesa *et al.,* 2019; Salas and Guimerà, 1996) (Figs. 2B; 3). The two studied sections belong to the Aguilón sub-basin, controlled by NW-SE oriented extensional faults (Aurell *et al.,* 2019) (Fig. 2B). In this sub-basin, after a long-lasting episode of non-deposition (latest Kimmeridgian to middle Valanginian), sedimentation resumed with the deposition of up to 300m of a Lower Cretaceous (mid-Valanginian to lower Barremian) syn-rift continental succession (Villanueva the Huerva and Aguilón formations; Cortés *et al.,* 1999; Soria et al., 1995) (Figs. 2C; 3). Subsiding areas were located SW of the Aguilón fault system and Villanueva de Huerva monocline (Cortés *et al.,* 1999) (Fig. 2C). The Tosos sector belonged to the subsiding area southwest of the Aguilón fault system, and consequently a thick (180m) succession of mid-Valanginian to lower Barremian deposits accumulated over the Higueruelas Fm. By contrast, the Fuendetodos sector was located on the non-subsiding area, NE of the Villanueva de Huerva monocline, therefore lacking the mid-Valanginian to lower Barremian sedimentary record (Figs. 2C; 3). After deposition of the Lower Cretaceous units, there was a major erosive and non-depositional gap until the deposition of syn-tectonic (Alpine) continental Cenozoic units (Paleocene to middle Miocene) (compressional stage in Fig. 3), with an interval of non-deposition and/or erosion from the latest Paleocene to early Oligocene (Cortés *et al.,* 1999). Around Tosos, this set of Cenozoic units is up to 600m thick (Pérez *et al.,* 1985; Pérez, 1989). However, the Fuendetodos sector was close to an Alpine structure

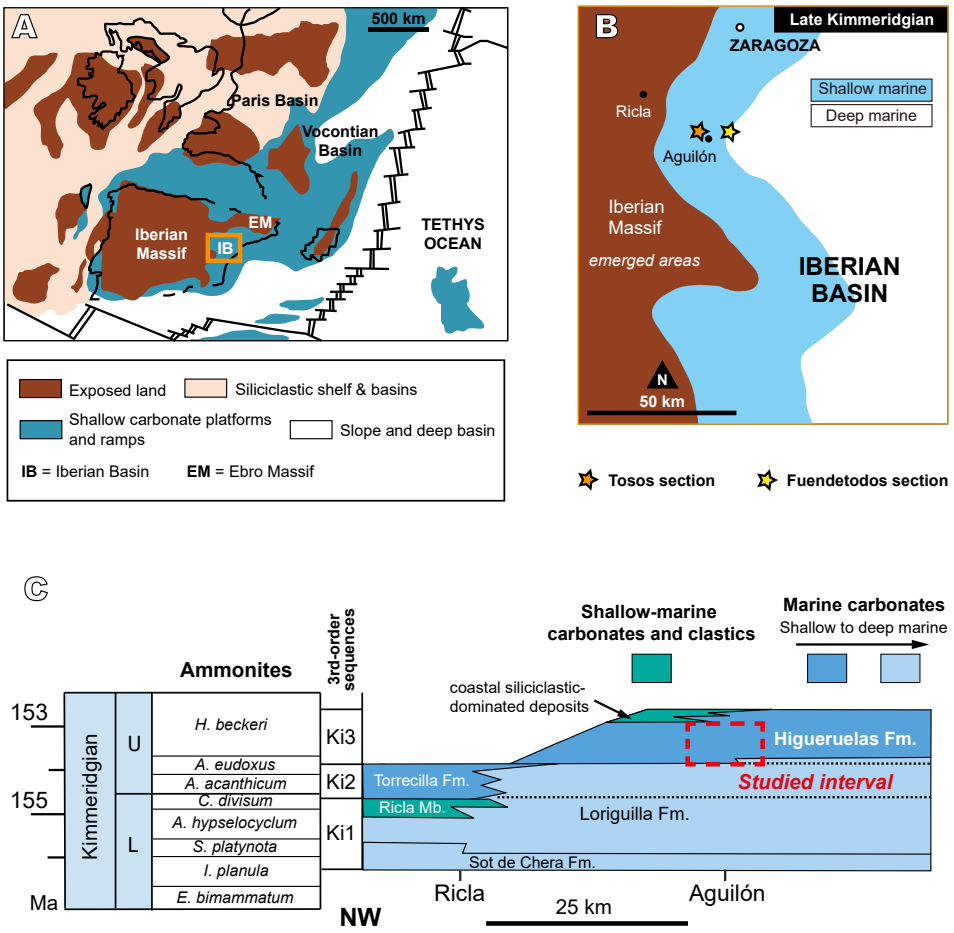

FIGURE 1. A) Palaeogeography of western Europe during the Late Jurassic, with the location of the Iberian Basin (modified from Dercourt *et al.*, 1993). B) Main facies belts in the Iberian Basin during the late Kimmeridgian (square in A) and location of the studied sections (south of the city of Zaragoza, NE Spain; compiled from Aurell *et al.*, 2003 and Ipas *et al.*, 2004). C) Kimmeridgian stratigraphy in the northern Iberian Basin (modified from Aurell *et al.*, 2019). The Higueruelas Fm., which is represented by the long-term third-order sequence Ki3, overlies open-marine marlstone and lime mudstone of the Loriguilla Fm., which is in turn laterally equivalent to the shallow-marine carbonates of the Higueruelas Fm. in eastern areas of the northern Iberian Basin (*i.e.* deep-marine areas in B).

(Mezalocha anticline) that represented a palaeo-high that remained exposed until the onset of the Miocene (Fig. 2C), and thus was mainly subjected to erosion and/or non-deposition during this stage (Fig. 3). In particular, around Fuendetodos, the Higueruelas Fm. is only overlain by a c. 200m-thick succession of middle Miocene lacustrine carbonates (Pérez *et al.*, 1985; Pérez, 1989).

In summary, the Higueruelas Fm. underwent a different burial and uplift history in the two studied sectors. In Tosos, these carbonate deposits were buried by at least 780m of lower Cretaceous (180m thick) and Cenozoic (600m thick) continental deposits, and affected by three intervals of non-deposition and/or erosion from the latest Kimmeridgian to middle Valanginian, from the middle Barremian to Paleocene, and from the latest Paleocene to early Oligocene (Fig. 3). In contrast, Fuendetodos remained mostly exposed from the latest Kimmeridgian to the middle Miocene, and only a 200m-thick continental succession is known to have been deposited over this section during the Cenozoic (Alpine) compressional stage. Even though other episodes of burial may have occurred in Fuendetodos from the latest Kimmeridgian to the middle Miocene, erosion and/or non-deposition associated with tectonic uplift dominated. In addition, on the basis of the previous stratigraphic framework established in this region (Sequero *et al.*, 2019), the upper part of the Higueruelas Fm. in the Fuendetodos sector is eroded (Fig. 3), lacking the last two high-frequency sequences (8 and 9) recognized in nearby distal sections.

STUDIED SUCCESSIONS AND SEDIMENTOLOGICAL FRAMEWORK

The uppermost Kimmeridgian Higueruelas Fm. studied in Tosos and Fuendetodos sections is 71m and 52m thick,

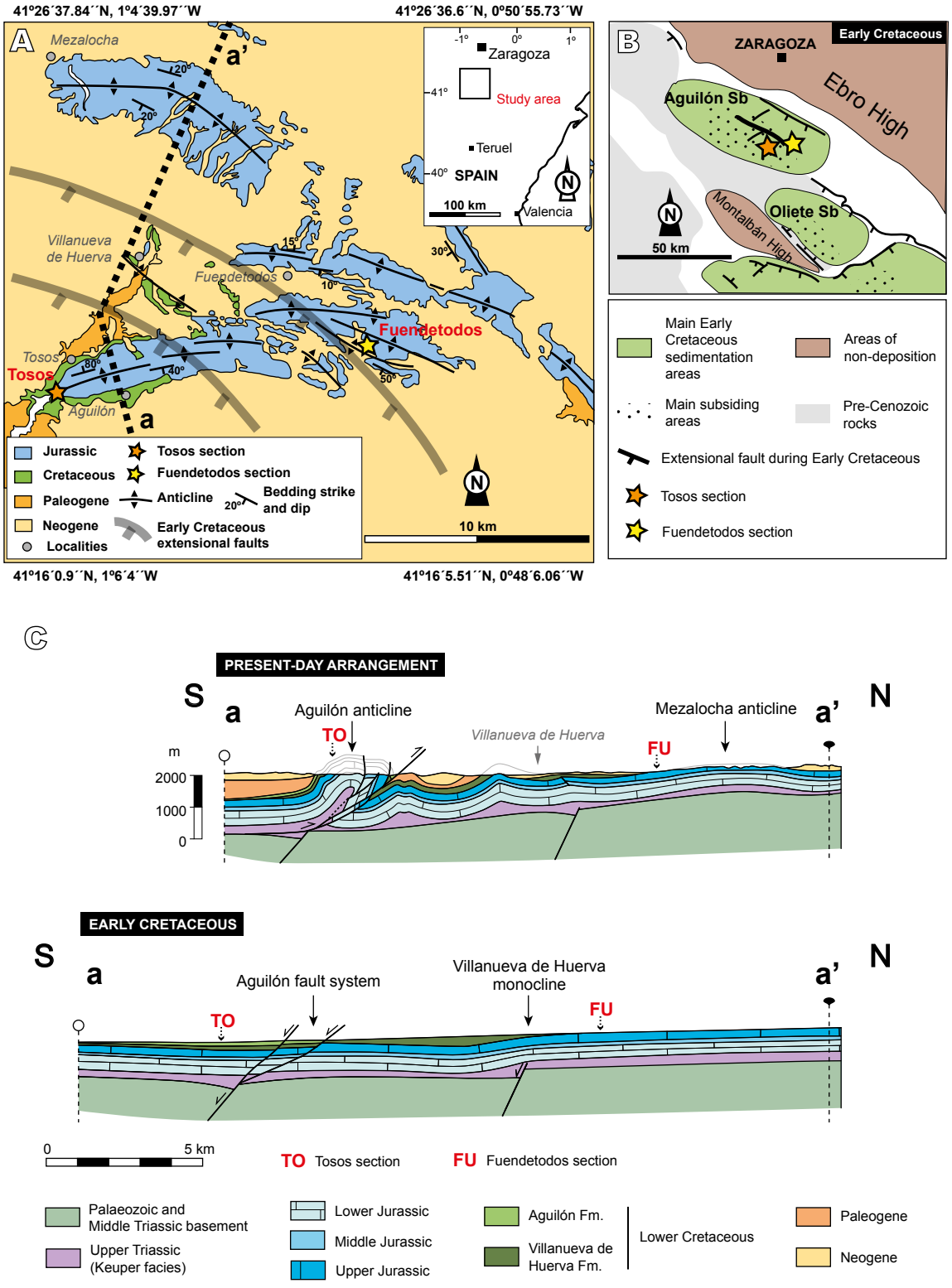

FIGURE 2. A) Extent of the Jurassic outcrops in the study area with the position of the studied logs (stars) and the cross-section a-a' shown in (C). The position of the Early Cretaceous extensional faults is included (grey colour) (modified from Cortés Gracia and Casas Sainz, 1996). B) Main sedimentation areas and active faults during the Late Jurassic-Early Cretaceous rifting episode in the northern Iberian Basin. The studied sections (stars) are situated in the newly formed Aguilón sub-basin (Aguilón Sb) (modified from Liesa *et al.*, 2019). C) Balanced cross-section (present-day arrangement) and suggested section restored to the top of the syn-rift sequence (Early Cretaceous) for the transect a-a' indicated in (A). The position of Tosos (TO) and Fuendetodos (FU) sections are included (modified from Cortés *et al.*, 1999).

respectively. These successions encompass high-frequency sequences 1 to 7 (in Tosos) and 2 to 7 (in Fuendetodos), and include a total of 14 facies representing deposition from inner-ramp domains (intertidal, lagoon, backshoal and shoal-sand blanket), mainly recorded in the Tosos section, to mid-ramp foreshoal and offshore areas represented in the Fuendetodos section (Sequero *et al.*, 2019, 2020) (Figs. 4; 5). Distance between the two sections, without restoring tectonic shortening, is around 15km (Fig. 5). Some decimetre- to metre-thick beds of totally or partially dolomitized facies are also recorded in both sections (Fig. 5), which post-date the deposition of the Higueruelas Fm. The origin of this replacive dolomitization has been related to circulation of hydrothermal fluids through faults during the Cenozoic Alpine compression, which acted as extensional faults during the Late Jurassic-Early Cretaceous rifting stage (Aurell, 1990) (Fig. 2C). However, it is also probable that these dolomites formed through fault-related hydrothermal circulation during the rifting episode, as similarly described in later studies about the Late Jurassic-Early Cretaceous dolomites in eastern areas of the Iberian Basin (*i.e.* Maestrat Basin; Travé *et al.*, 2019).

The detailed sedimentological framework of the studied successions is described in Sequero *et al.* (2019). Log correlation was based on the recognition of a number of well-marked bedding surfaces, which allowed the recognition of the high-frequency sequences 1 to 7

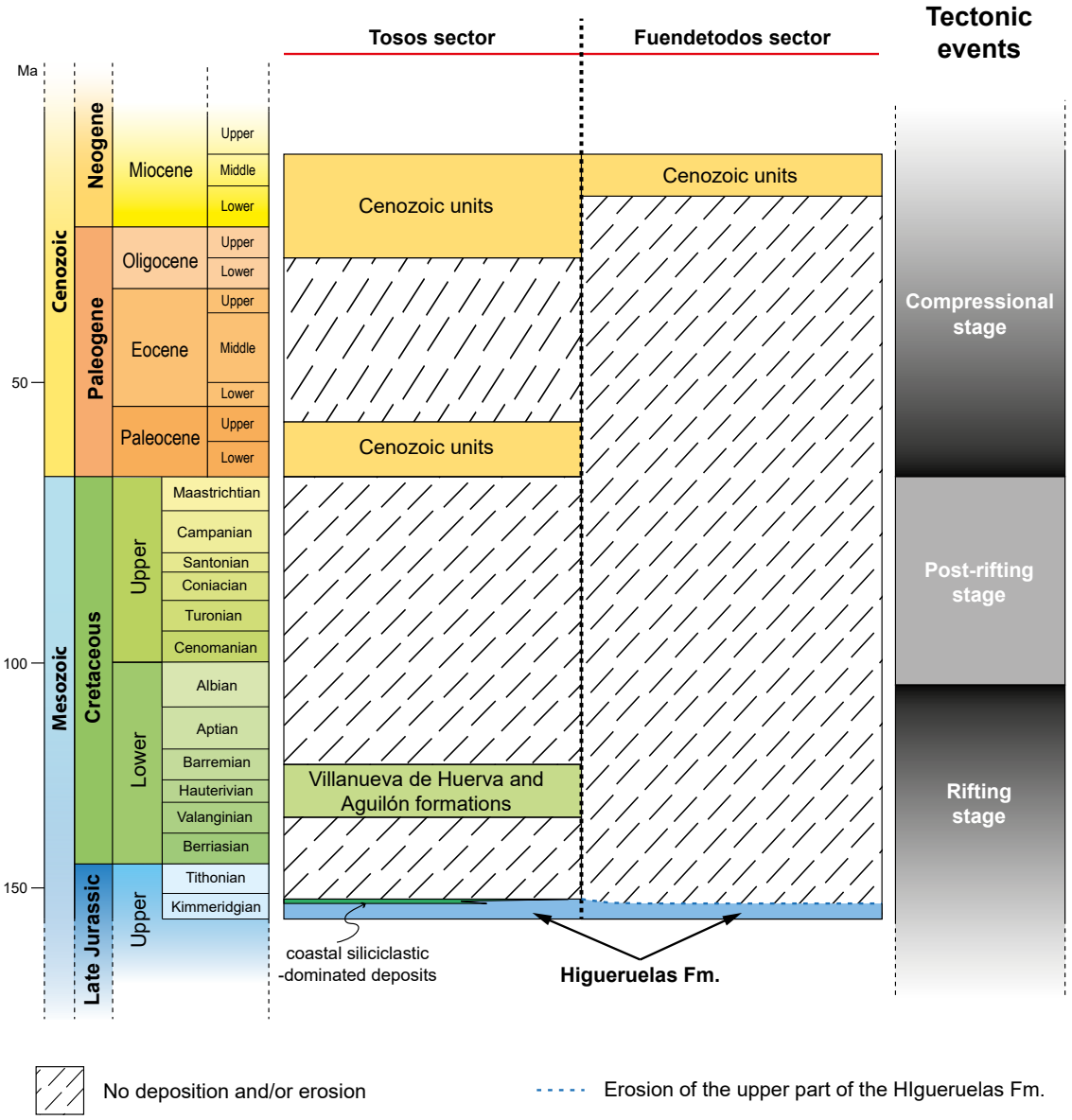

FIGURE 3. Stratigraphic record of the Tosos and Fuendetodos sectors from the Kimmeridgian to the middle Miocene, in relation to the tectonic stages of the Iberian Basin (based on Cortés *et al.*, 1999).

identified in these sections (Figs. 4; 5), and represent sedimentary discontinuities related to short-term sea-level fluctuations (*i.e.* short-term eccentricity cycles). These bedding planes are planar surfaces, some of which show bioturbation or Fe-encrustations, and locally represent hardgrounds. The high-frequency sequences 1 to 7 identified in the proximal Tosos section represent a complete record of the Higueruelas Fm. in this sector, with the boundaries with the underlying Loriguilla Fm. and the overlying carbonate-siliciclastic unit being distinguished in the field (Fig. 1C). However, the record of the upper part of the Higueruelas Fm. (*i.e.* sequences 8 and 9 recognized in nearby distal sections) is not preserved in the southeast, i.e. the distal Fuendetodos sector, due to the erosive gap related to the tectonic uplift in this part of the basin (Figs. 2C; 3). In both sections, there is no evidence of subaerial exposure at sequence boundaries that could be associated with the high-frequency sea-level fluctuations (*e.g.* Strasser, 2015), and at the top there is no record of latest Kimmeridgian karst or palaeosol formation.

A best-fit correlation between the discontinuity surfaces in the Tosos and Fuendetodos areas was performed, as no physical tracing between isolated outcrops was possible. This correlation is supported by the physical tracing of these sharp bedding planes along continuous outcrops of the Higueruelas Fm. in the same area (see Sequero *et al.,* 2018). This best-fit correlation was also constrained by the vertical facies evolution observed in the successive high-frequency sequences defined in these and other individual logs analysed in this region. Variable vertical facies trends are described for these sequences (shallowing, deepening, aggradational or deepening-shallowing) (Fig. 5), also varying from one section to another, since the local factors operating on the carbonate ramp strongly controlled the distribution and lateral migration of the facies types (Sequero *et al.,* 2019).

In the proximal Tosos section, the long-term shallowing-upward trend at the end of the Kimmeridgian is reflected by the evolution from mid-ramp facies (peloidal, peloidal-bioclastic and oncolitic wackestone-packstone) in sequence 1, to inner-ramp deposits (oolitic, peloidal-oolitic and oncolitic packstone-grainstone and stromatoporoid-rich facies) from the upper part of sequence 1 to sequence 5; and to restricted lagoonal facies (peloidal, bioclastic and oolitic packstone with local sandstone and marlstone) in sequences 5 to 7 (Fig. 5). In the relatively distal Fuendetodos section, the long-term shallowing-upward trend is recorded by the evolution from mid-ramp (offshore) peloidal and bioclastic wackestone-packstone alternating with chaetetid-stromatoporoid-coral-rich buildup and inter-buildup facies in sequences 2 to 5, to mid-ramp (foreshoal) peloidal, inter-buildup and oncolitic packstone-grainstone in sequences 6 and 7.

METHODOLOGY

Petrographic characterization

A total of 72 samples in thin sections, already used for differentiating depositional facies by Sequero *et al.* (2019), was analysed for the petrographic descriptions of facies under the binocular microscope, in particular differentiating between primary sedimentary carbonate components (*i.e.* micrite matrix and carbonate grains) from diagenetic calcite cements. Dolomitized facies (Fig. 5) have not been included in this work, since only a few totally or partially dolomitized beds occur in both sections. Nomenclature for calcite cements follows the terminology based on crystal fabric summarised in Flügel (2004).

Petrographic analysis was complemented by CathodoLuminescence (CL) microscopy on 21 thin sections (7 in Tosos and 14 in Fuendetodos), with a Technosyn Cold Cathodo Luminoscope, operating under 10-14kV beam potential, 0.5μA beam current and a 0.05-0.1 Torr pressure. CL analyses were used to characterize the primary carbonate components and calcite cements, on the basis of the absence or type of luminescence, as traditionally followed in the literature (Hiatt and Pufahl, 2014; Machel, 1985; Richter *et al.,* 2003; Savard *et al.,* 1995).

Carbon and oxygen stable isotope analyses

The carbon and oxygen stable isotope analyses were performed on the 72 bulk-rock samples collected in Tosos (n= 35) and Fuendetodos (n= 37) sections, and on calcitic shells from three specimens of *Trichites* (large-sized bivalve with very thick outer shell wall, proposed as reliable proxy for Jurassic pristine stable carbon and oxygen isotopic signature; cf. Zuo *et al.,* 2018) found in the offshore-proximal peloidal-bioclastic wackestone facies within sequence 2 of the Fuendetodos section (Fig. 5). In addition, two calcite veins found in the offshore-proximal peloidal-bioclastic packstone facies within sequence 5 of the Fuendetodos section were also analysed. Only two samples of calcite vein were analysed due to the difficulties in finding those veins with a suitable width to sample without contamination from the surrounding material. In order to ensure the reliability of the carbon and oxygen stable isotope compositions of each sample, a double measure per sample was carried out, giving a total of 173 stable isotope analyses (n= 77 in Tosos section, and n= 96 in Fuendetodos section) (see Table 1).

For the carbon and oxygen stable isotope analyses of bulk-rock samples, carbonate powders were extracted using a handheld micro-drill, avoiding calcite cements, calcite filled fractures and large bioclastic fragments of corals or stromatoporoids, due to the disequilibrium-isotopic precipitation by organisms (McConnaughey, 1989a, b).

TABLE 1. Carbon and oxygen stable isotope values (‰ V-PDB) from Tosos and Fuendetodos sections. Samples Tosos (TO) and Fuendetodos (FU) refer to bulk-carbonate samples in Tosos and Fuendetodos sections, respectively; samples TR refer to the calcitic bivalve shells of the three specimens of *Trichites* collected in the lower part of the Fuendetodos section, and samples CV to the calcite veins analysed in the upper part of the Fuendetodos section. A, B: double measure per sample; A-r, B-r: repeated measures every 10 analyses (the position of these repeated analyses does not appear consecutively in the table, as the isotopic measurements were not taken following the order of sample number). Std. Dev.: Standard deviation

Sample	$\delta^{18}O$	$\delta^{13}C$	Sample	$\delta^{18}O$	$\delta^{13}C$	Sample	$\delta^{18}O$	$\delta^{13}C$		$\delta^{18}O$	$\delta^{13}C$
Tosos section											
TO-1-A	-4.1	2.3	TO-13-A	-4.9	1.0	TO-24-B	-3.7	1.6			
TO-1-B	-4.1	2.2	TO-13-B	-5.3	0.8	TO-25-A	-3.9	1.4			
TO-2-A	-4.2	2.1	TO-14-A	-4.9	0.7	TO-25-B	-3.9	1.4			
TO-2-B	-4.1	2.1	TO-14-B	-4.9	0.8	TO-26-A	-3.3	1.5			
TO-3-A	-4.1	1.9	TO-15-A	-5.5	-0.9	TO-26-B	-3.2	1.2			
TO-3-B	-5.6	1.5	TO-15-A-r	-5.4	-0.9	TO-27-A	-4.5	0.4			
TO-4-A	-5.4	1.1	TO-15-B	-5.9	-1.4	TO-27-B	-4.4	0.4			
TO-4-B	-5.4	1.3	TO-16-A	-5.1	0.4	TO-28-A	-3.3	1.5			
TO-4-B-r	-5.3	1.3	TO-16-B	-5.2	0.2	TO-28-B	-3.1	1.4			
TO-5-A	-5.1	1.1	TO-17-A	-5.6	-0.3	TO-28-B-r	-3.1	1.4	Minimum	-7.1	-3.5
TO-5-B	-5.1	1.0	TO-17-B	-5.8	-0.6	TO-29-A	-4.6	0.5	Maximum	-2.4	2.3
TO-6-A	-4.5	1.3	TO-18-A	-5.4	0.0	TO-29-B	-4.5	0.6	Mean	-4.4	0.9
TO-6-B	-4.8	0.9	TO-18-B	-5.4	0.0	TO-30-A	-2.8	1.2	Std. Dev.	1.0	1.0
TO-7-A	-4.6	1.3	TO-19-A	-4.0	0.8	TO-30-B	-3.0	1.1			
TO-7-B	-4.7	1.3	TO-19-B	-4.1	0.7	TO-31-A	-2.4	1.5			
TO-8-A	-4.5	1.5	TO-20-A	-3.5	1.6	TO-31-B	-2.4	1.3			
TO-8-B	-4.4	1.3	TO-20-A-r	-3.6	1.6	TO-32-A	-2.9	1.3			
TO-9-A	-4.7	1.6	TO-20-B	-3.9	1.5	TO-32-B	-2.8	1.2			
TO-9-B	-4.5	1.7	TO-21-A	-3.6	1.9	TO-33-A	-2.7	0.7			
TO-10-A	-5.2	1.1	TO-21-B	-4.1	1.7	TO-33-B	-2.9	0.8			
TO-10-B	-5.4	1.0	TO-22-A	-7.0	-3.1	TO-34-A	-2.7	0.3			
TO-11-A	-4.9	1.1	TO-22-B	-7.1	-3.5	TO-34-A-r	-2.7	0.3			
TO-11-B	-5.0	0.8	TO-23-A	-4.6	1.7	TO-34-B	-3.2	0.2			
TO-12-A	-5.5	0.8	TO-23-B	-4.6	1.7	TO-35-A	-3.9	-0.1			
TO-12-B	-5.3	0.6	TO-23-A-r	-4.5	1.7	TO-35-B	-3.9	0.2			
TO-12-B-r	-5.3	0.6	TO-24-A	-3.4	1.6						
Fuendetodos section											
FU-1-A	-6.5	-5.6	FU-12-B	-4.7	-1.4	FU-24-B	-4.9	-0.3			
FU-1-B	-6.1	-5.1	FU-13-A	-4.8	-1.7	FU-25-A	-5.2	-1.3			
FU-1-B-r	-6.1	-5.0	FU-13-B	-4.5	-1.1	FU-25-B	-5.3	-1.4	Minimum	-6.6	-5.6
FU-2-A	-4.6	-2.0	FU-14-A	-6.2	-1.7	FU-26-A	-4.7	0.0	Maximum	-3.5	1.0
FU-2-A-r	-4.7	-2.1	FU-14-B	-6.1	-1.5	FU-26-B	-5.0	-0.2	Mean	-5.3	-1.4
FU-2-B	-5.8	-2.1	FU-15-A	-5.4	-0.6	FU-27-A	-5.2	-0.8	Std. Dev.	0.7	1.2
FU-3-A	-4.9	-0.8	FU-15-A-r	-5.6	-0.7	FU-27-B	-5.1	-0.6			
FU-3-B	-5.4	-1.4	FU-15-B	-5.6	-0.8	FU-28-A	-4.7	-0.1			
FU-4-A	-5.5	-2.3	FU-15-B-r	-5.5	-0.8	FU-28-B	-4.9	0.1	*Trichites*		
FU-4-B	-4.9	-0.9	FU-16-A	-5.9	-1.5	FU-29-A	-4.6	0.3	TR-1-A	-2.4	2.4
FU-5-A	-4.8	-0.4	FU-16-B	-6.0	-1.5	FU-29-B	-4.6	0.4	TR-1-A-r	-2.6	2.4
FU-5-B	-5.1	-0.5	FU-17-A	-6.3	-2.3	FU-30-A	-5.5	-1.1	TR-1-B	-2.3	2.5
FU-6-A	-4.6	-1.1	FU-17-B	-6.6	-2.5	FU-30-B	-4.8	-0.7	TR-1-B-r	-2.2	2.4
FU-6-B	-3.7	-0.2	FU-18-A	-5.7	-2.0	FU-31-A	-5.3	-2.5	TR-2-A	-3.4	1.4
FU-7-A	-4.5	-0.9	FU-18-B	-5.7	-2.0	FU-31-B	-5.2	-2.4	TR-2-B	-3.6	1.3
FU-7-A-r	-4.4	-0.9	FU-19-A	-5.9	-1.9	FU-32-A	-4.0	0.0	TR-3-A	-4.8	2.2
FU-7-B	-4.4	-1.1	FU-19-B	-5.8	-2.1	FU-32-B	-3.9	0.0	TR-3-B	-4.7	2.3
FU-8-A	-5.4	-1.5	FU-20-A	-5.4	-2.1	FU-33-A	-3.5	0.9	TR-3-B-r	-4.6	2.4
FU-8-B	-5.4	-1.4	FU-20-B	-5.3	-1.6	FU-33-B	-3.6	0.9			
FU-8-B-r	-5.5	-1.5	FU-21-A	-5.1	-1.4	FU-34-A	-6.1	-2.1			
FU-9-A	-5.5	-1.1	FU-21-B	-4.8	-0.7	FU-34-B	-6.1	-1.8	Calcite veins		
FU-9-B	-5.2	-0.2	FU-22-A	-5.8	-1.0	FU-35-A	-6.6	-3.8	CV-1-A	-7.7	-7.7
FU-10-A	-6.0	-2.4	FU-22-A-r	-5.8	-1.0	FU-35-B	-6.5	-3.5	CV-1-B	-7.7	-7.7
FU-10-B	-6.2	-2.7	FU-22-B	-5.5	-1.0	FU-36-A	-6.3	-2.9	CV-2-A	-7.3	-6.3
FU-11-A	-5.6	-1.3	FU-22-B-r	-5.7	-1.0	FU-36-B	-6.2	-2.9	CV-2-B	-7.5	-6.6
FU-11-B	-4.7	-0.9	FU-23-A	-5.8	-1.2	FU-37-A	-6.2	-3.1			
FU-11-B-r	-4.6	-0.8	FU-23-B	-5.9	-1.2	FU-37-B	-5.5	-2.9			
FU-12-A	-4.9	-1.5	FU-24-A	-4.9	0.1						

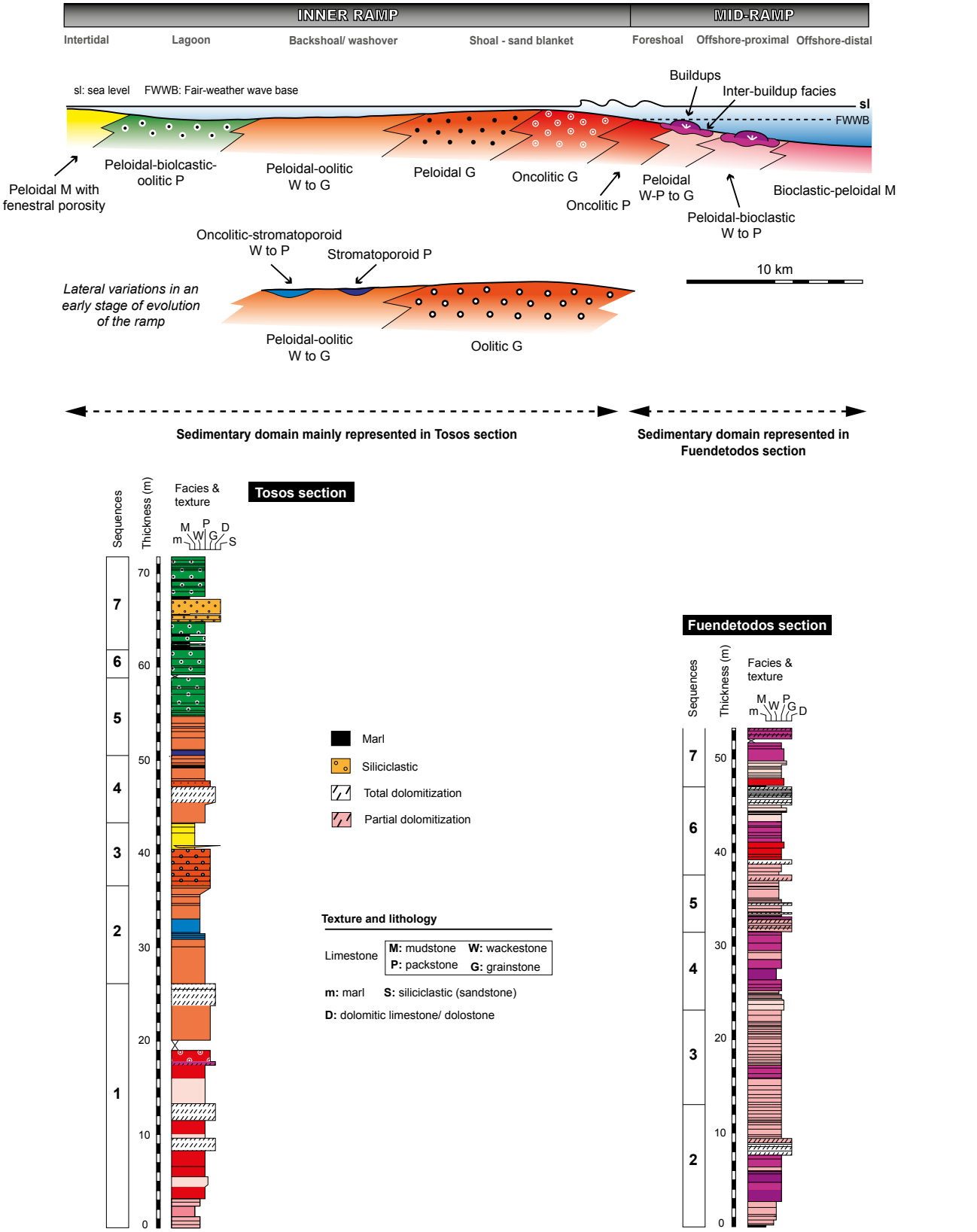

FIGURE 4. Sedimentary model of the latest Kimmeridgian shallow carbonate ramp and sedimentary logs of the Tosos and Fuendetodos sections. The Tosos section records deposition mainly in the inner-ramp domain, whereas the Fuendetodos section represents deposition in the middle ramp. Facies descriptions and interpretations are based on Sequero *et al.* (2019).

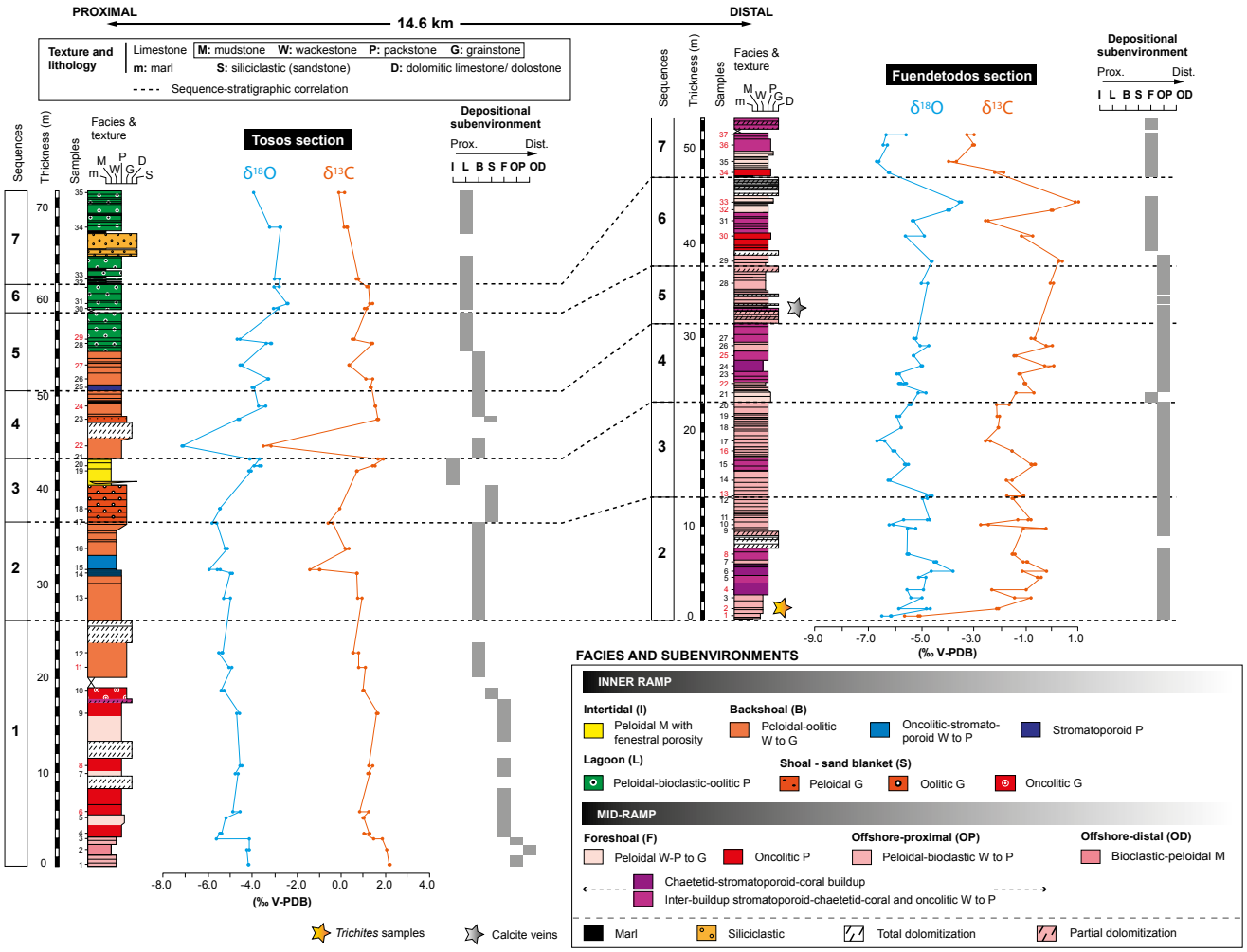

FIGURE 5. Sedimentary logs and carbon and oxygen stable isotope results plotted against stratigraphy of the Tosos and Fuendetodos sections, including the sequence-stratigraphic correlation based on Sequero *et al.* (2019). Samples in red colour include cathodoluminescence observations. The location of the *Trichites* samples and calcite veins analysed is also indicated (yellow and grey stars, respectively). Facies descriptions and interpretations are based on Sequero *et al.* (2019).

However, the incorporation of a certain amount of calcite cements filling the intraparticle or mouldic space of skeletal debris, interparticle spaces, and some fenestral pores, was in some cases inevitable. Isotope analyses of the interparticle or fenestral cement could not be performed in view of the difficulties in sampling without contamination from surrounding micrite or carbonate grains.

The carbon and oxygen stable isotope analyses were performed using an automated carbonate preparation device (GasBench II) connected to a Delta V Advantage (Thermo Fisher Scientific Inc.) isotope ratio mass spectrometer at the Earth Sciences Department, University of Milan (Italy). Carbonate powders were reacted with >99% orthophosphoric acid at 70ºC. The carbon and oxygen stable isotope compositions are expressed in the conventional delta notation calibrated to the Vienna Pee-Dee Belemnite (V-PDB) scale by the international standards IAEA-603 and NBS-18 and an internal laboratory standard. Analytical reproducibility for these analyses, being checked by repeated analyses of the certified carbonate standards, was better than ±0.1‰ for both $\delta^{13}C$ and $\delta^{18}O$ values.

RESULTS

Petrographic and cathodoluminescence analyses

The bulk-carbonate samples analysed from both the Tosos and Fuendetodos sections include a wide variety of primary carbonate components in variable proportions, mainly micrite matrix, peloids, ooids, oncoids and skeletal debris, as well as calcite cements filling mouldic vugs (generated by dissolution of skeletal debris), intraparticle and interparticle pores, fenestral pores and fissures (Figs. 6; 7). Local stylolites also occur in both sections.

Three types of calcite cement fabric have been recognized in all the investigated facies: granular, drusy and blocky. Granular to drusy calcite cements tend to fill mouldic, intraparticle and interparticle porosity. They generally constitute less than 10% of the thin-section area and are formed by anhedral to subhedral equant (granular, <10μm in size) and non-equigranular (drusy, 10 to 30μm in size) crystals (Figs. 6A-C; 7A-D). In the drusy calcite cements, crystal size increases towards the centre of the void (Fig. 6B). In some grainstone and packstone facies, granular and drusy interparticle cement follow the formation of elongated grain contact and mechanical compaction (Figs. 6C; 7C). Blocky calcite cements precipitated in fenestral pores, in rectilinear fissures (*i.e.* calcite veins; Fig. 6D) and locally in mouldic vugs (Fig. 7B). They constitute <10% of the thin-section area, and are formed by anhedral to subhedral crystals from hundreds of μm to several mm in size.

The proportion of primary sedimentary carbonate components and diagenetic calcite cements varies per facies type. In offshore mudstone to packstone and intertidal mudstone facies, peloids and micrite matrix constitute the main analysed components, with calcite cements representing <10% of the total volume of the sample, filling interparticle (in packstone) and intraparticle spaces, fenestral pores, mouldic vugs and/or rectilinear fissures (Fig. 6A, D). For lagoonal, backshoal and foreshoal wackestone to packstone facies, samples are mainly composed of variable proportions of micrite matrix, peloids, ooids and oncoids, as well as calcite cements mainly filling interparticle (in packstone), intraparticle and mouldic pores (Figs. 6C; 7A, B, D). These calcite cements constitute <10% of the total volume of the samples, locally 15% in backshoal oncolitic-stromatoporoid wackestone to packstone facies. However, for the backshoal, shoal-sand blanket and foreshoal grainstone facies (with peloids, ooids and/or oncoids), the proportion of calcite cements is higher (around 15% of the total volume) (Figs. 6B; 7C).

Primary carbonate components in most of the samples show no luminescence under CL (Figs. 6A'-D'; 7A'-D'), or locally dull (red or yellow) luminescence. Granular (GCC) to drusy (DCC) Calcite Cements filling mouldic, intraparticle and interparticle pores commonly show from no luminescence (GCC and locally DCC; Fig. 6A', C'; Fig. 7A', B', D') to dull (red or yellow) luminescence (DCC; Figs 6B', 7C'). Blocky Calcite Cements (BCC) display zoned (dark-yellow nuclei evolving into bright or dull-yellow rims) or no luminescence filling veins (zoned luminescence in Fig. 6D'), and dull (yellow) or no luminescence in interparticle spaces and mouldic vugs (Fig. 7B').

Carbon and oxygen stable isotope records

Carbon and oxygen stable isotope records for the Tosos and Fuendetodos sections are represented in Figure 5, and the values are listed in Table 1. The double measure per sample (labelled A and B following sample name in the table) confirms the consistency of the carbon and oxygen stable isotope composition obtained for each analytical point, with a mean reproducibility of ±0.2‰ for both $\delta^{13}C$ and $\delta^{18}O$ values.

The bulk $\delta^{13}C$ and $\delta^{18}O$ values of the inner-ramp Tosos succession range between -3.5 to 2.3‰ for $\delta^{13}C$ and -7.1 to -2.4‰ for $\delta^{18}O$ (Fig. 8), with a mean value of 0.9‰ and -4.4‰, respectively (standard deviation of 1‰ for both $\delta^{13}C$ and $\delta^{18}O$). In general, this section shows low-amplitude fluctuations for both $\delta^{13}C$ and $\delta^{18}O$ records, in the order of ≤1‰ with respect to the mean values (Fig. 5). In some cases, there are negative shifts in the order of 2‰ for the $\delta^{13}C$ record in the backshoal oncolitic-stromatoporoid wackestone-packstone facies within sequence 2 (at 31.5m), and in the order of 3-4‰ in both $\delta^{13}C$ and $\delta^{18}O$ values for backshoal peloidal-oolitic packstone facies at the onset of sequence 4 (at 44.5m).

The bulk $\delta^{13}C$ and $\delta^{18}O$ values along the mid-ramp Fuendetodos succession vary between -5.6 to 1.0‰ and -6.6 to -3.5‰, respectively (Fig. 8), with a mean value of -1.4‰ for $\delta^{13}C$ and -5.3‰ for $\delta^{18}O$ (standard deviation of 1.2‰ for $\delta^{13}C$ and 0.7‰ for $\delta^{18}O$), thus reflecting a general ^{13}C and ^{18}O depletion compared to the Tosos section. In addition, both $\delta^{13}C$ and $\delta^{18}O$ values show slightly higher-amplitude oscillations than in Tosos, in the order of 1-2‰ (Fig. 5). Two pronounced excursions with respect to the mean values are reported for the $\delta^{13}C$ record, accompanied by a coupled and less pronounced shift in the $\delta^{18}O$ values: a negative excursion at the onset of sequence 2 (at 0.5m) within offshore-proximal peloidal-bioclastic wackestone facies, with a deviation in the order of 3‰ for $\delta^{13}C$ and 1‰ for $\delta^{18}O$, and a positive shift in sequence 6 (at 44.5m), coinciding with deposition of foreshoal peloidal grainstone facies, being the $\delta^{13}C$ and $\delta^{18}O$ values deviated in the order of 3 and 2‰, respectively. The isotopic signals of the three specimens of *Trichites* collected in the lower part of this section show higher $\delta^{13}C$ values but a wider range for the $\delta^{18}O$ signature (Fig. 8), ranging between 1.3 to 2.5‰ for $\delta^{13}C$ and -4.8 to -2.2‰ for $\delta^{18}O$. The two analysed calcite veins show instead the lowest carbon and oxygen isotope values, ranging between -7.7 to -6.3‰ for $\delta^{13}C$ and -7.7 to -7.3‰ for $\delta^{18}O$ (Fig. 8).

The bulk carbon and oxygen stable isotope stratigraphy in both sections reveals no distinctive long-term $\delta^{13}C$ and $\delta^{18}O$ patterns, and the $\delta^{13}C$ and $\delta^{18}O$ trends observed within time-equivalent high-frequency sequences vary significantly from one section to the other (Fig. 5). Moreover, the bulk isotopic stratigraphy shows that the $\delta^{13}C$ and $\delta^{18}O$ values fluctuate in covariance, the degree of such $\delta^{18}O$-$\delta^{13}C$ covariance being relatively lower in

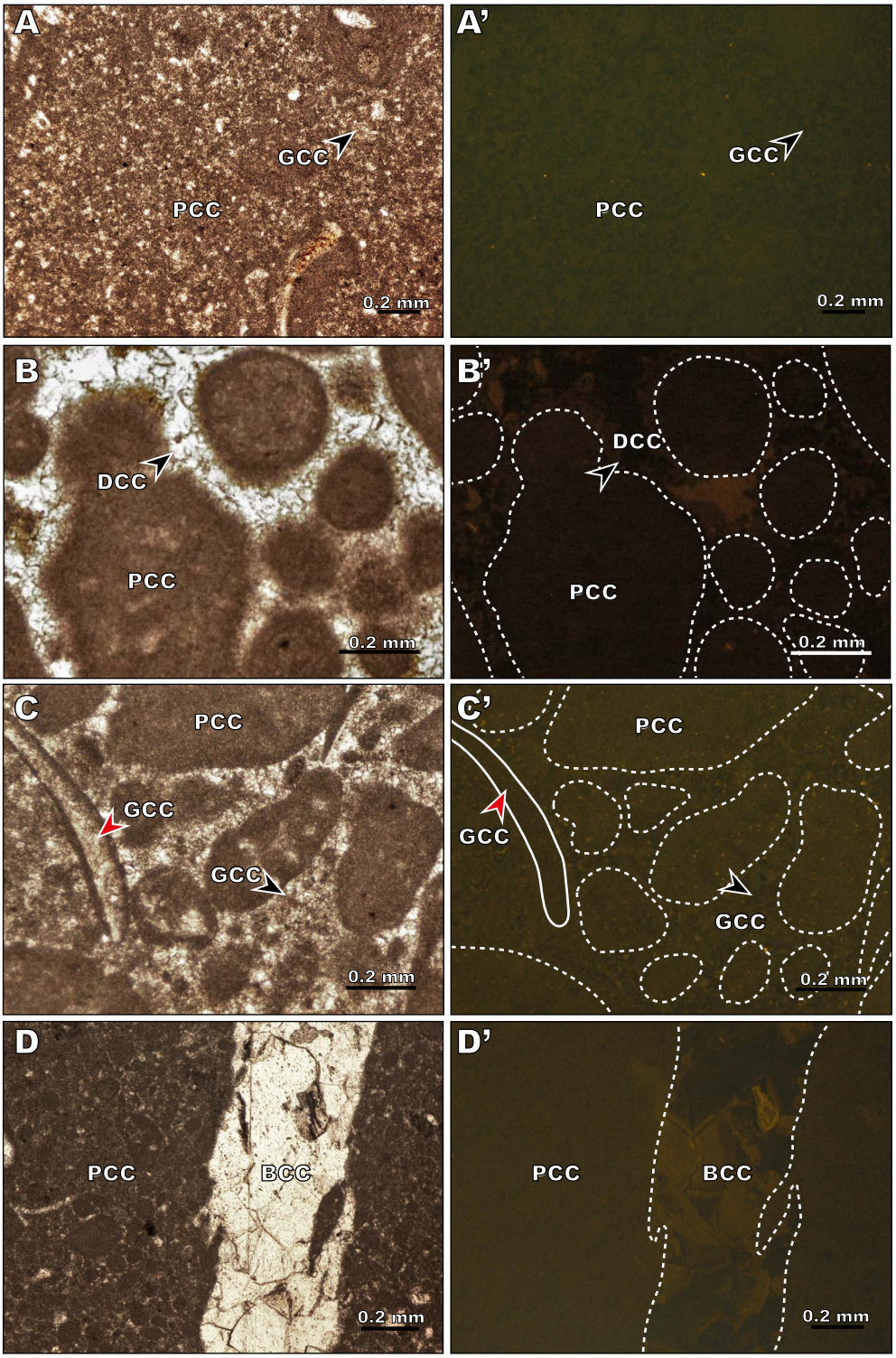

FIGURE 6. A-D) Polarized-light and A'-D') cathodoluminescence microphotographs of Primary Carbonate Components (PCC) and calcite cements (GCC: Granular Calcite Cement; DCC: Drusy Calcite Cement; BCC: Blocky Calcite Cement) from the Fuendetodos section. The micrite matrix, peloids, ooids and some skeletal grains show no luminescence (A'-D'; the main primary carbonate components are indicated with dashed lines in B' and C'), whereas the calcite cements display from no to dull (red or yellow) or zoned luminescence: A-A') GCC filling interparticle pores (arrows) with no luminescence; B-B') DCC in interparticle pores (arrows) with dull (red) luminescence; C-C') GCC in bioclastic vugs (red arrows) and interparticle pores (black arrows) with no luminescence. Notice that this cement follows the formation of elongated grain contact; D-D') BCC filling a rectilinear fissure, showing zoned (dark nuclei evolving into yellow rims) luminescence. A-A') Sample 1, offshore-proximal peloidal-bioclastic wackestone; B-B') sample 33, foreshoal peloidal grainstone; C-C') sample 36, foreshoal inter-buildup stromatoporoid-chaetetid-coral and oncolitic packstone; D-D') sample 25, offshore-proximal inter-buildup stromatoporoid-chaetetid-coral and oncolitic packstone.

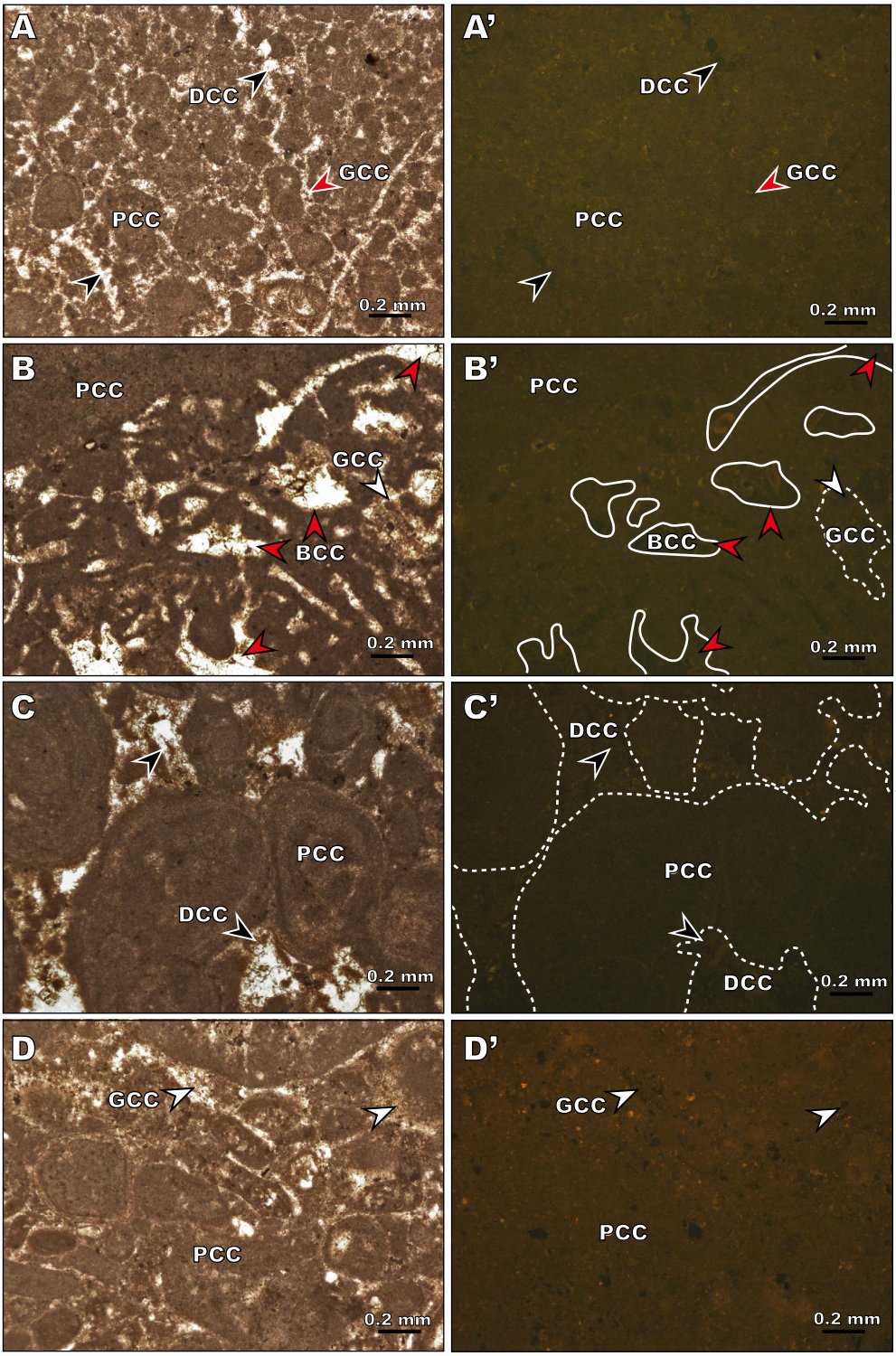

FIGURE 7. A-D) Polarized-light and A'-D') cathodoluminescence microphotographs of Primary Carbonate Components (PCC) and Calcite Cements (GCC: Granular Calcite Cement; DCC: Drusy Calcite Cement; BCC: Blocky Calcite Cement) from the Tosos section. The micrite matrix and other carbonate components (peloids, ooids, skeletal grains; A-D) show no luminescence (A'-D'; the main primary carbonate components are indicated with dashed lines in C'), whereas the calcite cements display from no to dull (red or yellow) luminescence: A-A') DCC and GCC (black and red arrows, respectively) in interparticle pores with no luminescence; B-B') BCC and GCC (red and white arrows, respectively) filling mouldic vugs (BCC), interparticle pores (BCC) and probable bioturbation galleries (GCC), showing no to locally dull (yellow) luminescence; C-C') DCC (black arrows) in interparticle pores with dull (red) luminescence. Notice that this cement follows mechanical compaction; D-D') GCC (white arrows) filling interparticle pores with no luminescence; A-A') Sample 6, foreshoal oncolitic packstone; B-B') sample 8, foreshoal oncolitic packstone; C-C') sample 11, backshoal peloidal-oolitic grainstone; D-D') sample 27, backshoal peloidal-oolitic packstone.

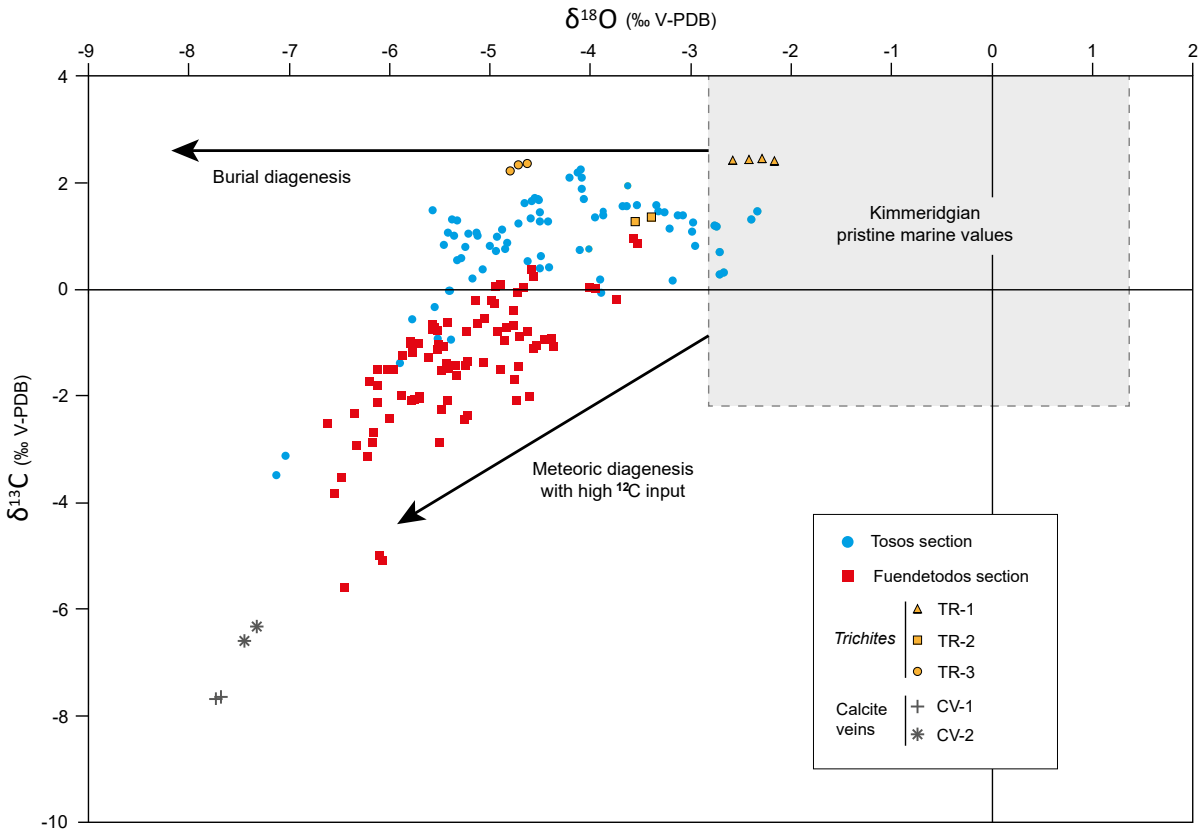

FIGURE 8. Scatter ($\delta^{18}O$, $\delta^{13}C$) diagram comparing the analysed bulk carbonates in the Tosos and Fuendetodos sections, including the isotopic composition of the calcitic bivalve shells from the three specimens of *Trichites* collected in the lower part of the Fuendetodos section (samples TR-1 to TR-3), and the isotopic composition of the two calcite veins analysed in the upper part of the Fuendetodos section (samples CV-1 and CV-2). The field of Kimmeridgian pristine marine values is based on the compilation of the stable isotope compositions obtained from well-preserved fossils (mainly belemnites) in Riboulleau *et al.* (1998), Jenkyns *et al.* (2002), Wierzbowski (2004) and Nunn and Price (2010). Trajectories indicating isotopic fields of carbonates influenced by burial and meteoric diagenesis are indicated, the latter incorporating high organic ^{12}C content from soil (based on Lavastre *et al.*, 2011).

Tosos (r^2= 0.29) but moderate in Fuendetodos (r^2= 0.52) (Fig. 9). In addition, the cross-plots of the bulk $\delta^{13}C$ and $\delta^{18}O$ values per facies types in each section do not show differentiated isotopic composition patterns regarding the facies type (Fig. 9), with the exception of the restricted lagoon peloidal-bioclastic-oolitic packstone facies in the Tosos section, which shows higher $\delta^{18}O$ values compared to the rest of the facies (Fig. 9A).

INTERPRETATION AND DISCUSSION

Diagenetic features from petrographic and cathodoluminescence analyses

The information obtained from the petrographic and cathodoluminescence analyses provides relevant data to evaluate the variable diagenetic features in the Tosos and Fuendetodos sections, and contributes to the interpretation of the stable isotope data. The analysed facies are predominantly wackestone to packstone accumulated in protected or below effective wave base depositional settings (Fig. 4). In view of the general low to moderate energy depositional domains, none of the investigated facies shows the presence of early marine cement in the form of isopachous rims of fibrous or radial fibrous cement (Figs. 6; 7).

The variable luminescence observed in the carbonates provides information about the redox conditions during precipitation of calcite (Barnaby and Rimstidt, 1989; Carpenter and Oglesby, 1976; Frank *et al.*, 1982; Machel, 1985; Oglesby, 1976). Luminescence is a common indicator of the incorporation of Mn^{2+} within the crystal lattice during water-rock interactions under suboxic to anoxic (generally burial) conditions (Flügel, 2004; Hiatt and Pufahl, 2014; Machel, 1985; Marshall, 1992; Richter *et al.*, 2003; Savard *et al.*, 1995). The absence of luminescence can in turn be attributed to both the absence of Mn^{2+} in the diagenetic fluids, precipitation under oxidizing conditions, or the incorporation of Fe^{2+} under reducing conditions, since Fe^{2+} is a common quencher resulting in dull or no luminescence

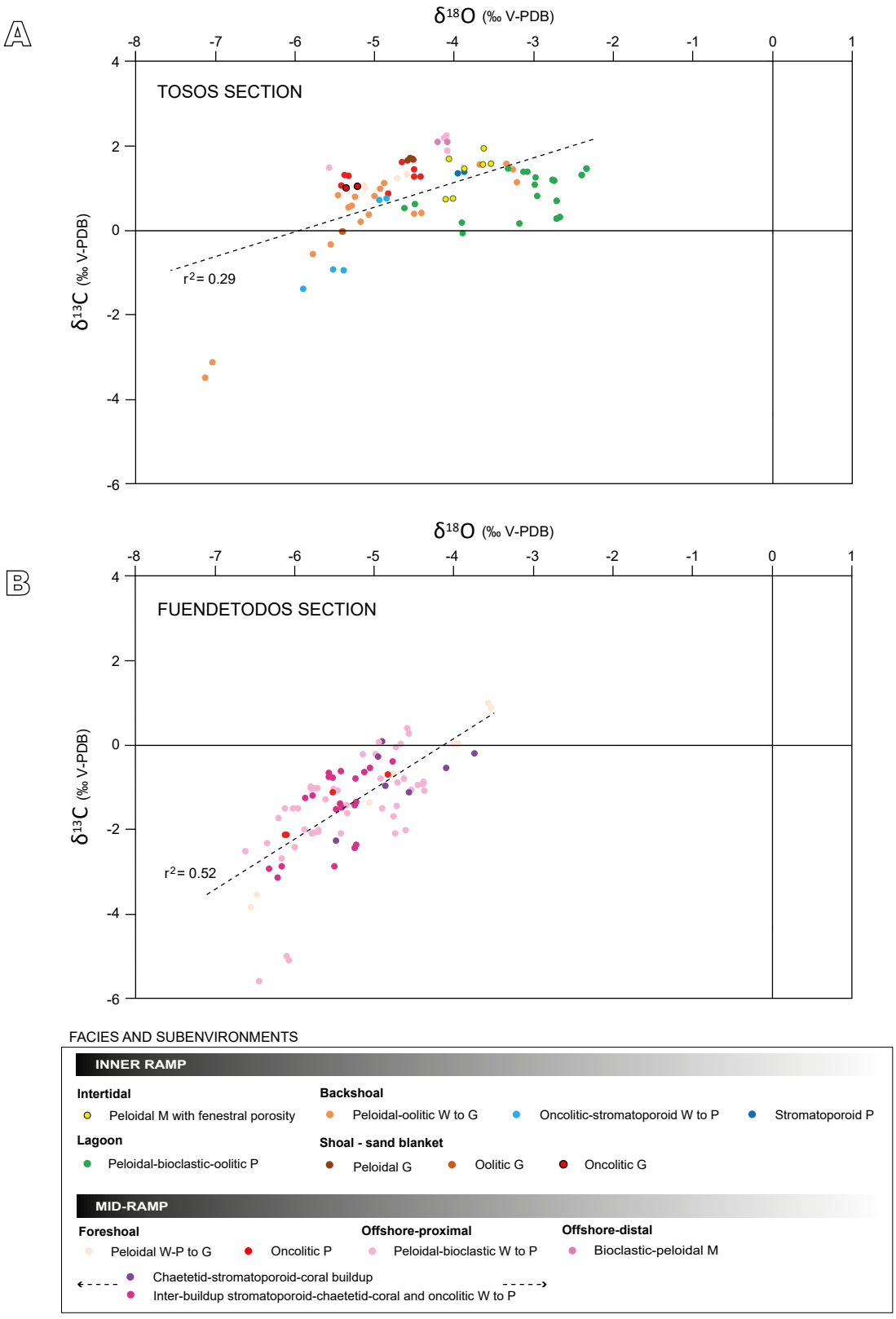

FIGURE 9. Cross-plots of $\delta^{13}C$ and $\delta^{18}O$ values of the analysed bulk carbonates in A) Tosos and B) Fuendetodos sections according to the facies type. The $\delta^{18}O$-$\delta^{13}C$ covariance is relatively low in the Tosos section (r^2= 0.29), but moderate in the Fuendetodos section (r^2= 0.52). The scatter of the $\delta^{13}C$ and $\delta^{18}O$ data for both sections does not show distinct patterns regarding the facies type, with the exception of the restricted lagoon peloidal-bioclastic-oolitic packstone facies in the Tosos section (A).

(Flügel, 2004; Hiatt and Pufahl, 2014; Machel, 1985; Marshall, 1992; Richter *et al.,* 2003; Savard *et al.,* 1995). Therefore, the dull (red or yellow) luminescence observed in drusy (DCC), blocky (BCC) and locally granular (GCC) calcite cements, filling intraparticle and interparticle spaces, mouldic vugs and fissures, suggests precipitation under reducing burial conditions (mesogenesis). The non-luminescence could instead indicate precipitation in a meteoric phreatic diagenetic setting during uplift after burial (telogenesis) (cf. Flügel, 2004 and references therein) (Figs. 6A'-C'; 7A'-D'). The zoned luminescence observed in some blocky (BCC) calcite cements filling fractures (Fig. 6D') suggests precipitation during burial in fluctuating redox conditions. The local presence of stylolites in both sections is also indicative of burial compaction. In this regard, granular (GCC) and drusy (DCC) calcite cements filling interparticle spaces in grainstone-packstone seem to post-date mechanical compaction, forming elongated and concavo-convex grain contacts (Figs. 6C; 7C).

Diagenetic alteration of carbon and oxygen stable isotope record

The scatter diagram for the measured bulk $\delta^{13}C$ and $\delta^{18}O$ values of the Tosos and Fuendetodos sections shows that diagenesis significantly modified the original isotopic signature of these uppermost Kimmeridgian shallow-marine carbonate deposits in both localities, although with distinctive differences in each section (Fig. 8).

Oxygen isotope values for bulk carbonates from Tosos (-7.1 to -2.4‰, with most of the values ranging between -5.9 to -2.4‰) and Fuendetodos (-6.6 to -3.5‰) are lower than those reported in the literature for pristine Kimmeridgian marine carbonates (between -2.8 to 1.4‰; *e.g.* Jenkyns *et al*., 2002; Nunn and Price, 2010; Riboulleau *et al.,* 1998; Wierzbowski, 2004) (Fig. 8). If these published pristine Kimmeridgian marine values are assumed valid for the Kimmeridgian shallow-water domains in the Iberian Basin, the different magnitudes of deviation in the Fuendetodos and Tosos sections can be used to discuss both the imprint of the diagenetic alteration and the origin of the diagenetic fluids. In particular, the deviation of the $\delta^{18}O$ values with respect to the pristine Kimmeridgian marine carbonates is higher in Fuendetodos than in Tosos, in the order of 1 to 3‰ for Tosos and of 2 to 3‰ for Fuendetodos (Fig. 8).

The variation for carbon isotope values also shows remarkable differences between both sections. In the Tosos section, the measured $\delta^{13}C$ values (-3.5 to 2.3‰, with most of the values ranging between -1.4 to 2.3‰) are similar to those published for pristine Kimmeridgian marine carbonates (between -2.3 to 4.7‰; Jenkyns *et al.,* 2002; Nunn and Price, 2010; Riboulleau *et al.,* 1998; Wierzbowski, 2004), whereas in Fuendetodos, measured $\delta^{13}C$ values (-5.6 to 1.0‰, with most of the values ranging between -3.8 to 0.3‰) are lower than those described in the literature, in the order of 3 to 4‰, suggesting a diagenetic overprint. Although during powder sampling for stable isotope analyses there was likely contamination of sedimentary components and diagenetic cements, samples from the two sections display different distinctive average stable isotope signatures and trends, which is indicative of resetting by different diagenetic processes and fluids.

The diagenetic alteration affecting the studied carbonate deposits overprinted a possible palaeoenvironmental signal from the isotopic record. The covarying $\delta^{13}C$ and $\delta^{18}O$ vertical trends in the Tosos and Fuendetodos sections can be interpreted as an indicator of this diagenetic resetting, as traditionally reported in the literature (Allan and Matthews, 1982; Fike *et al.,* 2006; Grotzinger *et al.,* 2011; Metzger and Fike, 2013). In recent studies (Swart and Oehlert, 2018), it has been suggested that such covariance is not a definitive marker of diagenetic alteration. However, in this case, this assumption can be considered since there is no other evidence in either the Tosos or Fuendetodos sections to support the preservation of a palaeoenvironmental signal from the isotopic record, such as: i) the absence of a facies-dependent pattern on the isotopic record which could be associated with changes in the depositional conditions (Colombié *et al.,* 2011; Immenhauser *et al.,* 2002, 2003; Patterson and Walter, 1994; Zuo *et al.,* 2018) (Fig. 9); ii) the absence of distinctive long-term variation patterns in the $\delta^{13}C$ and $\delta^{18}O$ stratigraphy (Fig. 5), showing only low-amplitude oscillations in both sections with local excursions, and iii) the highly varying vertical $\delta^{13}C$ and $\delta^{18}O$ trends observed within the time-equivalent high-frequency sequences from one section to another (Fig. 5), being not possible to establish a significance for these isotopic variations. The significance for the local excursions in the $\delta^{13}C$ and $\delta^{18}O$ values observed in both sections is also uncertain, as no other differences from the petrographic features are found compared to the rest of the samples.

The three specimens of *Trichites* collected from the Fuendetodos section have the potential to record the original latest Kimmeridgian seawater stable isotope composition, as reported by previous authors (Zuo *et al.,* 2018). Therefore, they could be used for quantifying the magnitude of the diagenetic resetting. However, the diagenetic overprint reported on the bulk carbonates in the studied sections can also be observed in the $\delta^{13}C$ and $\delta^{18}O$ values of the *Trichites* calcitic shells (Fig. 8). Sample TR-1 shows the closest $\delta^{18}C$ and $\delta^{18}O$ values to the pristine Kimmeridgian marine carbonates (a mean value of 2.4‰ for $\delta^{13}C$ and of -2.4‰ for $\delta^{18}O$; see Table 1), but they also fall within the range of those reported for the diagenetically altered bulk carbonates in the Tosos section. In addition, the two other specimens (samples TR-2 and TR-3) display a

higher deviation in the $\delta^{18}O$ signature, in the order of 1-2‰ with respect to the pristine Kimmeridgian marine values. Therefore, the $\delta^{13}C$ and $\delta^{18}O$ values of these specimens of *Trichites* seem to have also been diagenetically altered.

In the Fuendetodos section, the isotope signatures obtained from calcite veins (samples CV-1 and CV-2 in Fig. 8) confirm that the isotope data in this section gradually approach the low values of the late diagenetic calcite in fractures.

Comparison between Tosos-Fuendetodos: burial vs meteoric diagenetic alteration

The $\delta^{18}O$ record in the Tosos section, with most of the data points deviated towards very low $\delta^{18}O$ values (Fig. 8), is characteristic of closed high-temperature burial diagenetic systems (Banner and Hanson, 1990; van der Kooij *et al.,* 2009; Madden and Wilson, 2013; Marshall, 1992; Plunkett, 1997; Swart, 2015). Hot burial fluids in contact with carbonate rocks give rise to a depletion of ^{18}O in the $\delta^{18}O$ values, because of the high temperature-related fractionation of the oxygen stable isotope (Brand and Veizer, 1981; Immenhauser *et al.,* 2002; Lohmann, 1988; Magaritz, 1983; Marshall, 1992; Morse and MacKenzie, 1990). In contrast, the carbon stable isotope fractionation is less dependent on temperature, and in a closed system the dissolved inorganic carbon is provided by the host carbonate rock (Brand and Veizer, 1981; Lohmann, 1988; Marshall, 1992; Morse and MacKenzie, 1990). This fits with the $\delta^{13}C$ values in the Tosos section, being that these values are close to those of the pristine Kimmeridgian marine carbonates (Fig. 8). In contrast, the dispersion observed for the data in the Fuendetodos section, with significant lower $\delta^{13}C$ and $\delta^{18}O$ values, suggests a higher interaction with ^{18}O-depleted meteoric fluids incorporating organic ^{12}C probably derived from soil weathering (Allan and Matthews, 1982; Bahamonde *et al.,* 2017; Hudson, 1977; Immenhauser *et al.,* 2002; Lavastre *et al.,* 2011; Lohmann, 1988; Moore, 2001; O'Neil, 1987; Patterson and Walter, 1994; Vogel, 1993). The two calcite veins analysed in the Fuendetodos section (Fig. 8), showing the lowest $\delta^{13}C$ and $\delta^{18}O$ values compared to those reported for both the Tosos and Fuendetodos sections, reflect the isotopic signature of calcite likely precipitated from meteoric fluids (*e.g.* Hudson, 1977; Nelson and Smith, 1996) during telogenesis after tectonic uplift. In this regard, the proximity of the $\delta^{13}C$ and $\delta^{18}O$ values obtained in the Fuendetodos section to those reported for the calcite veins, confirms the pervasive diagenetic alteration of these limestones by meteoric fluids. This is also consistent with the higher and relatively significant $\delta^{18}O$-$\delta^{13}C$ covariance observed in Fuendetodos (r^2= 0.52) compared to Tosos (r^2= 0.29) (Fig. 9), highlighting a major resetting of the primary isotopic composition in Fuendetodos by meteoric fluids (Marshall, 1992; Rosales *et al.,* 2001; Swart, 2015; Swart and Oehlert, 2018; Veizer *et al.,* 1997).

The variable diagenetic overprint recorded on the isotopic composition in the Tosos and Fuendetodos sections is consistent with the different post-depositional processes occurring in this part of the Iberian Basin from the end of the Kimmeridgian. In Tosos, the uppermost Kimmeridgian carbonates of the Higueruelas Fm. studied here are overlain by a thick (up to 780m) continental succession deposited during the middle Valanginian to middle Miocene (Pérez *et al.,* 1985; Pérez, 1989; Soria *et al.,* 1995), with three long-lasting periods of subaerial exposure during the latest Kimmeridgian to middle Valanginian, from the middle Barremian to Paleocene and from the latest Paleocene to early Oligocene (Fig. 3). In contrast, the Fuendetodos sector remained mostly exposed due to tectonic uplift until the middle Miocene, and the Higueruelas Fm. is overlain by only a c. 200m-thick succession of middle Miocene lacustrine carbonates (Pérez *et al.,* 1985; Pérez, 1989). These specific post-depositional histories controlled different late-diagenetic processes affecting the uppermost Kimmeridgian deposits in both localities, as reflected on the isotopic record (Fig. 8). In the Tosos section, the Higueruelas Fm. was affected by a long period (from mid-Valanginian to mid-Miocene) of burial (negative deviation of $\delta^{18}O$, but not of $\delta^{13}C$ values, due to hot burial diagenetic fluids). However, these deposits in the Fuendetodos section were mainly subjected to uplift-related meteoric alteration (negative deviation of both $\delta^{18}O$ and $\delta^{13}C$ values).

Is diagenetic alteration dependent on facies type?

Palaeoenvironmental factors controlling sedimentation in the latest Kimmeridgian shallow carbonate ramp of the Iberian Basin are not reflected in the isotopic composition obtained from these carbonates in the Tosos and Fuendetodos sections, due to diagenetic resetting. Different diagenetic processes governing the post-depositional evolution of the Higueruelas Fm. have instead overprinted the primary marine $\delta^{13}C$ and $\delta^{18}O$ signature in each section. In this regard, considering the variability in the textural characteristics observed for the analysed deposits, the effect of the diagenetic alteration on the carbon and oxygen stable isotope records can be variable as a function of the depositional texture type. Accordingly, the coarser textures, with higher primary porosity and permeability, are more favourable for fluid circulation, which may result in a higher diagenetic overprint (Al-Mojel *et al.,* 2018; Coimbra *et al.,* 2014; Huck *et al.,* 2017; Immenhauser *et al.,* 2002; Marshall, 1992; Vincent *et al.,* 2004). Therefore, for the Higueruelas Fm., an approximation of the possible link between textural features and the degree of alteration of the primary isotopic signature has been attempted with the available data in Figure 10.

In Tosos, a variable response to the diagenetic alteration regarding the textural types can be appreciated (Fig. 10A). There is a particular difference in the isotopic composition scatter for the grainstone textures, showing the lowest $\delta^{13}C$ and $\delta^{18}O$ values compared to the other textures. In the Fuendetodos section, however, the diagenetic alteration indistinctly affected the carbonate deposits, not reporting differentiated $\delta^{13}C$ and $\delta^{18}O$ values regarding the textural type (Fig. 10B). This distinct pattern in the texture-diagenetic alteration relationship in the Tosos and Fuendetodos sections could be related to the different post-depositional processes affecting the Higueruelas Fm. at each locality. For the Tosos section, which underwent a long period of relatively shallow burial, it is probable that the diagenetic alteration predominantly reflects variable fluid-rock interaction depending on the porosity and

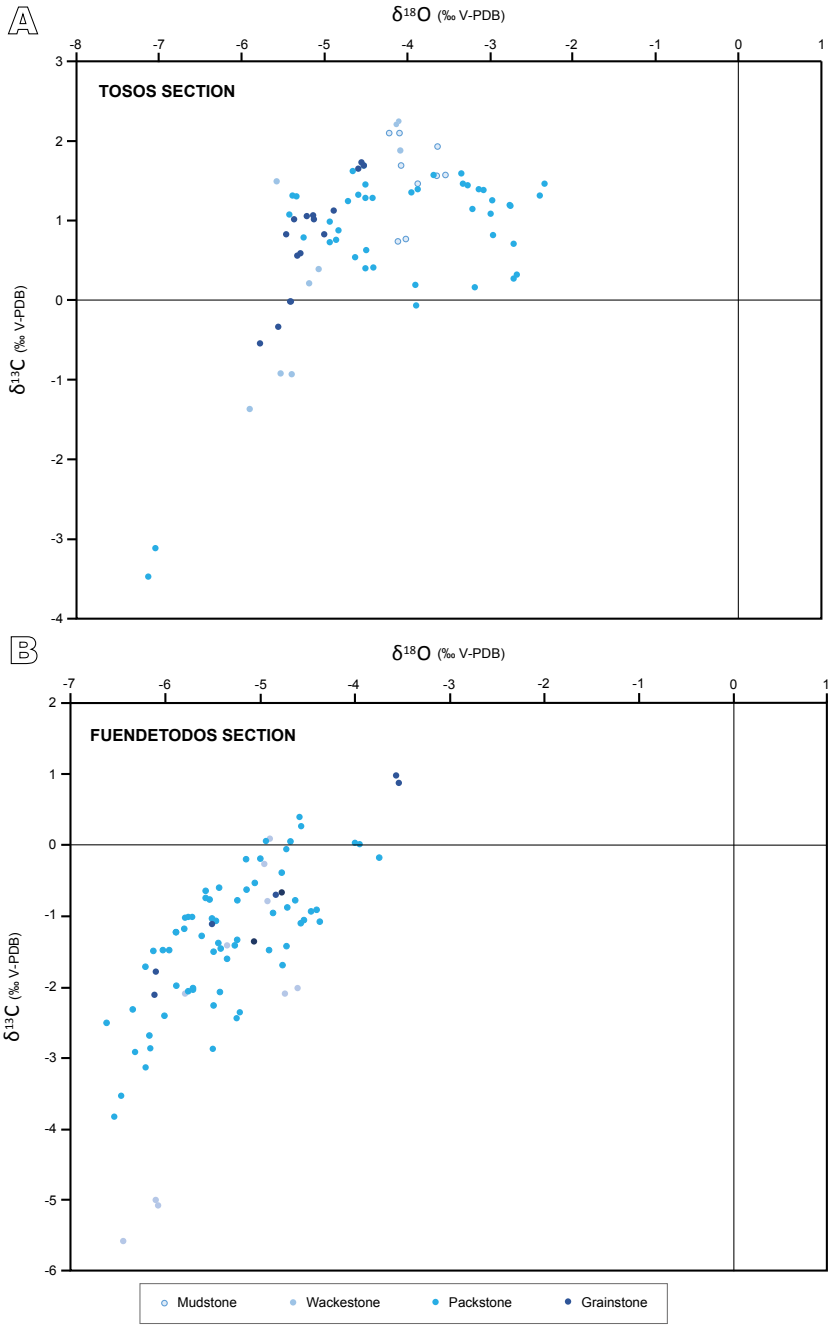

FIGURE 10. Cross-plots of $\delta^{13}C$ and $\delta^{18}O$ values of the analysed bulk carbonates in A) Tosos and B) Fuendetodos sections according to depositional textural types. For simplification, four categories of textures are indicated: mudstone, wackestone (including mudstone-wackestone), packstone (including wackestone-packstone) and grainstone (including packstone-grainstone). A relationship between the degree of diagenetic alteration and the texture type is observed in the Tosos section (A), but not in the Fuendetodos section (B).

permeability of the sediment, but also a variable degree of contamination by sampling burial cement. Most of the calcite cements incorporated during sampling correspond to granular (GCC) and drusy (DCC) calcite cements, which seem to have been precipitated as burial diagenetic phases, because they followed mechanical compaction and show dull luminescence (DCC; Fig. 6B'). In this sense, there is also a relationship between the amount of calcite cement precipitated and the alteration of the isotopic signature, the grainstone textures having a larger amount of burial calcite cement (around 15% of the total volume), compared to the rest of the textures (less than 10%). In contrast to this scenario, the Higueruelas Fm. in the Fuendetodos section was mostly uplifted (Figs. 2C; 3) and exposed to meteoric diagenesis during the long-term uplift from the latest Kimmeridgian to middle Miocene, and therefore to a probably more complex succession of diagenetic events (*i.e.* meteoric waters with variable chemical composition probably related to different climate and vegetation, or meteoric waters that interacted with different rocks in the phreatic zone), thus obliterating a texture-diagenetic alteration pattern. This is also supported by the higher diagenetic alteration reported for the Fuendetodos section (*i.e.* the lowest $\delta^{13}C$ and $\delta^{18}O$ values, close to the isotopic composition of the meteoric calcite veins) compared to the Tosos section.

A noteworthy aspect that arises from this study is that from the Fuendetodos section, which represents a deeper depositional environment, one would expect isotopic data less influenced by meteoric diagenesis. Instead, this section appears more altered by meteoric fluids than the Tosos section, which represents shallower-water domains. On the other hand, it is also remarkable that both sections, despite being governed by different diagenetic processes, show similar calcite cements in terms of fabrics and cathodoluminescence properties (Figs. 6A'-D'; 7A'-D'). These similarities, along with the diagenetic resetting revealed in each section, provide the background for further analyses in order to understand the imprint of specific burial and tectonic histories on the carbon and oxygen stable isotope data from these shallow-marine carbonates. On the other hand, the results obtained in this study can also be applied to similar cases in order to understand how the carbon and oxygen stable isotope signatures are altered in specific post-depositional contexts.

CONCLUSIONS

Bulk carbon and oxygen stable isotope compositions recorded in the uppermost Kimmeridgian shallow carbonate ramp deposits in the northern Iberian Basin (Higueruelas Fm., NE Spain), reveal the variable effect of burial and meteoric diagenesis (following tectonic uplift) in two selected sections (nearly 15km apart) representing the proximal (Tosos section) and relatively distal (Fuendetodos section) areas of the carbonate ramp.

This study reveals that the deeper-water facies, represented in the Fuendetodos section, are those more affected by meteoric alteration compared to the Tosos section, despite representing shallower-water domains. This particularity is a consequence of different burial and tectonic histories affecting the Higueruelas Fm. at each locality, which is reflected on the variable diagenetic resetting of the isotope data. In the Tosos section, the cross-plot of the bulk $\delta^{13}C$ and $\delta^{18}O$ values shows a significant decrease in the $\delta^{18}O$ signature compared with the pristine Kimmeridgian marine carbonates, but instead a similar carbon isotope composition. This type of diagenetic alteration results from a post-depositional evolution in a closed high-temperature burial system. In this area, the Higueruelas Fm. was affected by long-term (from Cretaceous to Miocene) burial, as these deposits are overlain by a c. 780m-thick continental succession deposited during the middle Valanginian to middle Miocene. On the contrary, the Higueruelas Fm. in the Fuendetodos section remained mostly exposed due to tectonic uplift, and was affected by meteoric diagenesis from the latest Kimmeridgian until the middle Miocene, recording a significant depletion of both ^{13}C and ^{18}O. In both sections, the strong influence exerted by the diagenetic resetting makes the $\delta^{13}C$ and $\delta^{18}O$ records unsuitable for addressing palaeoenvironmental reconstructions.

A relationship between the magnitude of the diagenetic alteration on the isotopic signature and the facies type is observed. In the Tosos section, the grainstone textures are those showing the lowest $\delta^{13}C$ and $\delta^{18}O$ values compared to the other textures. For the Fuendetodos section, however, no differentiated isotopic composition patterns regarding the textural types are observed. In contrast to the isotopic record, similar cement types in terms of fabrics and cathodoluminescence properties are reported in both sections.

This study highlights the importance of integrated studies (sedimentology, regional tectonic evolution and burial history, diagenesis) in order to better understand and interpret the carbon and oxygen stable isotope signature in ancient shallow-marine carbonates. In addition, the Tosos section shows a relationship between the textural types and the diagenetic alteration, but this does not occur in the Fuendetodos section, affected by a long-term uplift and exposure to meteoric fluids rather than burial. These results can be applied to similar cases in order to understand how the carbon and oxygen stable isotope signatures are altered in specific post-depositional contexts, and so provide the background for further investigations focused on the relationship between the fabric type and the magnitude

of the stable isotope resetting in those carbonates mainly affected by burial diagenesis.

ACKNOWLEDGMENTS

This work is part of the project CGL 2017-85038-P funded by MCIN/AEI/10.13039/501100011033 and "ERDF A way of making Europe". The research of Cristina Sequero is funded by a FPU Grant subsidized by the Spanish Ministry of Science and Innovation. We also appreciate the financial support provided by the International Association of Sedimentologists (IAS Postgraduate Grant Scheme) and the use of the Servicio General de Apoyo a la Investigación-SAI, Universidad de Zaragoza. The authors also gratefully acknowledge Idoia Rosales (Instituto Geológico y Minero de España, IGME) for the laboratory assistance in cathodoluminescence microscopy, and Ana Moreno (Instituto Pirenaico de Ecología, IPE, Spain) for providing the laboratory instruments for sampling.

REFERENCES

Allan, J.R., Matthews, R.K., 1982. Isotope signatures associated with early meteoric diagenesis. Sedimentology, 29, 797-817.

Al-Mojel, A., Dera, G., Razin, P., Le Nindre, Y-M., 2018. Carbon and oxygen isotope stratigraphy of Jurassic platform carbonates from Saudi Arabia: Implications for diagenesis, correlations and global paleoenvironmental changes. Palaeogeography, Palaeoclimatology, Palaeoecology, 511, 388-402.

Anderson, T.F., Arthur, M.A., 1983. Stable isotopes of oxygen and carbon and their application to sedimentologic and paleoenvironmental problems. In: Arthur, M.A., Anderson, T.F., Kaplan, I.R., Veizer, J., Land, L.S. (eds.). Stable Isotopes in Sedimentary Geology. Tulsa, Society of Economic Paleontologists and Mineralogists (SEPM), Short Course 10, 1-151.

Aurell, M., Meléndez, A., 1986. Sedimentología de la Formación Calizas con oncolitos de Higueruelas (Malm) en la región de Muel-Belchite (Provincia de Zaragoza). Acta Geológica Hispánica, 21-22, 307-312.

Aurell, M., 1990. El Jurásico Superior en la Cordillera Ibérica Central (provincias de Zaragoza y Teruel). Análisis de cuenca. Ph.D. Thesis. Zaragoza, University of Zaragoza, 534pp.

Aurell, M., Robles, S., Bádenas, B., Rosales, I., Quesada, S., Meléndez, G., García-Ramos, J.C., 2003. Transgressive-regressive cycles and Jurassic palaeogeography of northeast Iberia. Sedimentary Geology, 162, 239-271.

Aurell, M., Bádenas, B., Ipas, J., Ramajo, J., 2010. Sedimentary evolution of an Upper Jurassic epeiric carbonate ramp, Iberian Basin, NE Spain. In: Van Buchem, F.S.P., Gerdes, K.D., Esteban, M. (eds). Mesozoic and Cenozoic Carbonate Systems of the Mediterranean and the Middle East: Stratigraphic and Diagenetic Reference Models. Geological Society, London, Special Publications, 329, 89-111.

Aurell, M., Ipas, J., Bádenas, B., Muñoz, A., 2012. Distribución de facies con corales y estromatopóridos en el dominio interno de una plataforma carbonatada (Titónico, Cordillera Ibérica). Geogaceta, 51, 67-70.

Aurell, M., Bádenas, B., Canudo, J.I., Castanera, D., García-Penas, A., Gasca, J.M., Martín-Closas, C., Moliner, L., Moreno-Azanza, M., Rosales, I., Santas, L., Sequero, C., Val, J., 2019. Kimmeridgian-Berriasian stratigraphy and sedimentary evolution of the central Iberian Rift System (NE Spain). Cretaceous Research, 103, 104153.

Bádenas, B., Aurell, M., 2001. Kimmeridgian palaeogeography and basin evolution of northeastern Iberia. Palaeogeography, Palaeoclimatology, Palaeoecology, 168, 291-310.

Bádenas, B., Aurell, M., 2003. Análisis comparado y controles en la sedimentación de dos arrecifes de la zona media de una rampa carbonatada del Jurásico Superior de la Cordillera Ibérica. Revista de la Sociedad Geológica de España, 16(3-4), 151-166.

Bahamonde, J.R., Della Porta, G., Merino-Tomé, O.A., 2017. Lateral variability of shallow-water facies and high-frequency cycles in foreland basin carbonate platforms (Pennsylvanian, NW Spain). Facies, 63(2), 6.

Banner, J.L., Hanson, G.N., 1990. Calculation of simultaneous isotopic and trace element variations during water-rock interaction with applications to carbonate diagenesis. Geochimica et Cosmochimica Acta, 54(11), 3123-3137.

Barnaby, R.J., Rimstidt, J.D., 1989. Redox conditions of calcite cementation interpreted from Mn and Fe contents of authigenic calcites. Geological Society of America Bulletin, 101, 795-804.

Bartolini, A., Pittet, B., Mattioli, E., Hunziker, J.C., 2003. Shallow-platform palaeoenvironmental conditions recorded in deep-shelf sediments: C and O stable isotopes in Upper Jurassic sections of southern Germany (Oxfordian–Kimmeridgian). Sedimentary Geology, 160, 107-130.

Brand, U., Veizer, J., 1980. Chemical diagenesis of a multicomponent carbonate system -1: trace elements. Journal of Sedimentary Petrology, 50, 1219-1236.

Brand, U., Veizer, J., 1981. Chemical diagenesis of a multicomponent carbonate system -2: Stable isotopes. Journal of Sedimentary Petrology, 51, 987-997.

Brand, U., Posenato, R., Came, R., Affek, H., Angiolini, L., Azmy, K., Farabegoli, E., 2012. The end-Permian mass extinction: a rapid volcanic CO2 and CH4-climatic catastrophe. Chemical Geology, 322, 121-144.

Carpenter, A.B., Oglesby, T.W., 1976. A model for the formation of luminescently zoned calcite cements and its implications. Geological Society of America Abstracts with Programs, 8, 469-470.

Carpenter, S.J., Lohmann, K.C., 1989. $\delta^{18}O$ and $\delta^{13}C$ variations in Late Devonian marine cements from the Golden Spike and Nevis reefs, Alberta, Canada. Journal of Sedimentary Petrology, 59, 792-814.

Carpenter, S.J., Lohmann, K.C., 1997. Carbon isotope ratios of Phanerozoic marine cements: re-evaluating the global carbon

and sulfur systems. Geochimica et Cosmochimica Acta, 61, 4831-4846.

Castro, J.M., de Gea, G.A., Quijano, M.L., Aguado, R., Froehner, S., Naafs, B.D.A., Pancost., R.D., 2019. Complex and protracted environmental and ecological perturbations during OAE 1a – Evidence from an expanded pelagic section from south Spain (Western Tethys). Global and Planetary Change, 183, 103030.

Chung, H.M., Rooney, M.A., Toon, M.B., Claypool, G.E., 1992. Carbon isotope composition of marine crude oils. The American Association of Petroleum Geologists Bulletin, 76(7), 1000-1007.

Coimbra, R., Immenhauser, A., Olóriz, F., 2014. Spatial geochemistry of Upper Jurassic marine carbonates (Iberian subplate). Earth-Science Reviews, 139, 1-32.

Colombié, C., Lécuyer, C., Strasser, A., 2011. Carbon- and oxygen-isotope records of palaeoenvironmental and carbonate production changes in shallow-marine carbonates (Kimmeridgian, Swiss Jura). Geological Magazine, 148(1), 133-153.

McConnaughey, T.A., 1989a. 13C and 18O isotopic disequilibrium in biological carbonates: I. Patterns. Geochimica et Cosmochimica Acta, 53, 151-162.

McConnaughey, T.A., 1989b. ^{13}C and ^{18}O isotopic disequilibrium in biological carbonates: II. *In vitro* simulation of kinetic isotope effects. Geochimica et Cosmochimica Acta, 53, 163-171.

Cortés Gracia, A.L., Casas Sainz, A.M., 1996. Deformación alpina de zócalo y cobertera en el borde norte de la Cordillera Ibérica (Cubeta de Azuara-Sierra de Herrera). Revista de la Sociedad Geológica de España, 9(1-2), 51-66.

Cortés, A.L., Liesa, C.L., Soria, A.R., Meléndez, A., 1999. Role of extensional structures on the location of folds and thrusts during tectonic inversion (northern Iberian Chain, Spain). Geodinamica Acta, 12(2), 113-132.

Dercourt, J., Ricou, L., Vrielynck, B., 1993. Atlas: Tethys palaeoenvironmental Maps. Paris, Gauthier-Villars, 14pp.

Derry, L.A., 2010. A burial diagenesis origin for the Ediacaran Shuram-Wonoka carbon isotope anomaly. Earth and Planetary Science Letters, 294, 152-162.

Eltom, H.A., Gonzalez, L.A., Hasiotis, S.T., Rankey, E.C., Cantrell, D.L., 2018. Paleogeographic and paleo-oceanographic influences on carbon isotope signatures: Implications for global and regional correlation, Middle-Upper Jurassic of Saudi Arabia. Sedimentary Geology, 364, 89-102.

Fike, D.A., Grotzinger, J.P., Pratt, L.M., Summons, R.E., 2006. Oxidation of the Ediacaran Ocean. Nature, 444, 744-747.

Flügel, E., 2004. Microfacies of Carbonate Rocks. Analysis, Interpretation and Application. Germany,Springer-Verlag, 976pp.

Frank, J.R., Carpenter, A.B., Oglesby, T.W., 1982. Cathodoluminescence and composition of calcite cement in the Taum Sauk Limestone (Upper Cambrian), southeast Missouri. Journal of Sedimentary Petrology, 52, 631-638.

Given, R.K., Lohmann, K.C., 1985. Derivation of the original isotopic composition of Permian marine carbonates. Journal of Sedimentary Petrology, 55, 430-439.

Glumac, B., Walker, K., 1998. A Late Cambrian positive carbon-isotope excursion in the southern Appalachians: relation to biostratigraphy, sequence stratigraphy, environments of deposition, and diagenesis. Journal of Sedimentary Research, 68(6), 1212-1222.

Grötsch, H.J., Billing, I., Vahrenkamp, V., 1998. Carbon-isotope stratigraphy in shallow-water carbonates: implications for Cretaceous black-shale deposition. Sedimentology, 45, 623-634.

Grotzinger, J.P., Fike, D.A., Fischer, W.W., 2011. Enigmatic origin of the largest-known carbon isotope excursion in Earth's history. Nature Geoscience, 4, 285-292.

Guimerà, J., Álvaro, M., 1990. Structure et évolution de la compression alpine dans la Chaîne Ibérique et la Chaîne côtière catalane (Espagne). Bulletin de la Societé géologique de France, 6(2), 339-348.

Hiatt, E.E., Pufahl, P.K., 2014. Cathodoluminescence petrography of carbonate rocks: a review of applications for understanding diagenesis, reservoir quality, and pore system evolution. In: Coulson, I.M. (ed.). Cathodoluminescence and its application to geoscience. Mineralogical Association of Canada Short Course, 45, 75-96.

Huck, S., Wohlwend, S., Coimbra, R., Christ, N., Weissert, H., 2017. Disentangling shallow-water bulk carbonate carbon isotope archives with evidence for multi-stage diagenesis: An in-depth component-specific petrographic and geochemical study from Oman (mid-Cretaceous). The Depositional Record, 3, 233-257.

Hudson, J.D., 1977. Stable isotopes and limestone lithification. Journal of the Geological Society, 133(6), 637-660.

Immenhauser, A., Kenter, J.A.M., Ganssen, G., Bahamonde, J.R., Van Vliet, A., Saher, M.H., 2002. Origin and significance of isotope shifts in Pennsylvanian carbonates (Asturias, NW Spain). Journal of Sedimentary Research, 72(1), 82-94.

Immenhauser, A., Della Porta, G., Kenter, J.A., Bahamonde, J.R., 2003. An alternative model for positive shifts in shallow-marine carbonate $\delta^{13}C$ and $\delta^{18}O$. Sedimentology, 50(5), 953-959.

Ipas, J., Aurell, M., Bádenas, B., 2004. Ambientes sedimentarios y secuencias en la Fm. Higueruelas (Jurásico Superior) en la Cordillera Ibérica Septentrional. Geogaceta, 35, 7-10.

Jenkyns, H.C., Clayton, C.J., 1986. Lower Jurassic epicontinental carbonates and mudstones from England and Wales: chemostratigraphic signals and the early Toarcian anoxic event. Sedimentology, 44, 687-706.

Jenkyns, H.C., Jones, C.E., Gröcke, D.R., Hesselbo, S.P., Parkinson, D.N., 2002. Chemostratigraphy of the Jurassic System: applications, limitations and implications for palaeoceanography. London, Journal of the Geological Society, 159, 351-378.

Joachimski, M.M., 1994. Subaerial exposure and deposition of shallowing upward sequences: evidence from stable isotopes of Purbeckian peritidal carbonates (basal Cretaceous), Swiss and French Jura Mountains. Sedimentology, 41, 805-824.

van der Kooij, B., Immenhauser, A., Csoma, A., Bahamonde, J., Steuber, T., 2009. Spatial geochemistry of a Carboniferous platform-margin-to-basin transect: balancing environmental and diagenetic factors. Sedimentary Geology, 219, 136-150.

Lavastre, V., Ader, M., Buschaert, S., Petit, E., Javoy, M., 2011. Water circulation control on carbonate- $\delta^{18}O$ records in a low permeability clay formation and surrounding limestones: the Upper Dogger–Oxfordian sequence from the eastern Paris basin, France. Applied Geochemistry, 26(5), 818-827.

Lavoie, D., Bourque, P.A., 1993. Marine burial and meteoric diagenesis of early Silurian carbonate ramps, Quebec Appalachians, Canada. Journal of Sedimentary Petrology, 63(2), 233-247.

Liesa, C.L., Soria, A.R., Casas, A., Aurell, M., Meléndez, N., Bádenas, B., Fregenal-Martínez, M., Navarrete, R., Peropadre, C., Rodríguez-López, J.P., 2019. The South Iberian, Central-Iberian and Maestrazgo basins. In: Quesada, C., Oliveira, J.T. (eds.). The Geology of Iberia: A Geodynamic Approach Vol. 3. Springer Nature Switzerland AG, Alpine Cycle, 214-228.

Lohmann, K.C., 1988. Geochemical patterns of meteoric diagenetic systems and their application to studies of paleokarst. In: James, N.P., Choquette, P.W. (eds.). Paleokarst. Berlin, Springer-Verlag, 50-80.

Machel, H.G., 1985. Cathodoluminiscence in calcite and dolomite and its chemical interpretation. Geoscience Canada, 12(4), 139-147.

Madden, R., Wilson, M.E., 2013. Diagenesis of a SE Asian Cenozoic carbonate platform margin and its adjacent basinal deposits. Sedimentary Geology, 286-287, 20-38.

Magaritz, M., 1983. Carbon and oxygen isotope composition of recent and ancient coated grains. In: Peryt, T.M. (ed.). Coated Grains. Berlin, Springer-Verlag, 27-37.

Marshall, J.D., 1992. Climatic and oceanographic isotopic signals from the carbonate rock record and their preservation. Geological Magazine, 129, 143-160.

Metzger, J.G., Fike, D.A., 2013. Techniques for assessing spatial heterogeneity of carbonate $\delta^{13}C$ values: Implications for craton-wide isotope gradients. Sedimentology, 60, 1405-1431.

Moore, C.H., 1989. Carbonate Diagenesis and Porosity. Developments in Sedimentology Vol. 46. Amsterdam, Elsevier, 337pp.

Moore, C.H., 2001. Carbonate Reservoirs: Porosity evolution and diagenesis in a sequence stratigraphic framework. Amsterdam, Elsevier, 460pp.

Morse, J.W., Mackenzie, F.T., 1990. Geochemistry of sedimentary carbonates: Developments in Sedimentology, 48, 707pp.

Nelson, C.S., Smith, A.M., 1996. Stable oxygen and carbon isotope compositional fields for skeletal and diagenetic components in New Zealand Cenozoic nontropical carbonate sediments and limestones: a synthesis and review. New Zealand Journal of Geology and Geophysics, 39, 93-107.

Nunn, E.V., Price, G.D., 2010. Late Jurassic (Kimmeridgian-Tithonian) stable isotopes ($\delta^{18}O$, $\delta^{13}C$) and Mg/Ca ratios: New paleoclimate data from Helmsdale, northeast Scotland. Palaeogeography, Palaeoclimatology, Palaeoecology, 292, 325-335.

Oehlert, A.M., Swart, P.K., 2019. Rolling window regression of $\delta^{13}C$ and $\delta^{18}O$ values in carbonate sediments: Implications for source and diagenesis. The Depositional Record, 5(3), 613-630.

Oglesby, T.W., 1976. A model for the distribution of manganese, iron and magnesium in authigenic calcite and dolomite cements in the Upper Smackover Formation in eastern Mississippi. PhD Thesis. University of Missouri, 122pp.

O'Neil, J.R., 1977. Stable isotopes in mineralogy. Physics and Chemistry of Minerals, 2, 105-123.

O'Neil, J.R., 1987. Preservation of H, C, and O isotopic ratios in the low temperature environment. In: Kyser, T.K. (ed.). Stable Isotope Geochemistry of Low Temperature Fluids. Mineralogical Association of Canada, Saskatoon, 85-128.

Patterson, W.P., Walter, L.M., 1994. Depletion of ^{13}C in seawater ΣCO_2 on modern carbonate platforms: Significance for the carbon isotopic record of carbonates. Geology, 22, 885-888.

Peckmann, J., Thiel, V., 2004. Carbon cycling at ancient methane-seeps. Chemical Geology, 205(3-4), 443-467.

Pérez, A., Azanza, B., Cuenca, G., Pardo, G., Villena, J., 1985. Nuevos datos estratigráficos y paleontológicos sobre el Terciario del borde meridional de la depresión del Ebro (provincia de Zaragoza). Estudios Geológicos, 41, 405-411.

Pérez, A., 1989. Estratigrafia y sedimentologia del Terciario del borde meridional de la Depresión del Ebro (sector riojano-aragonés) y cubetas de Muniesa y Montalban. PhD Thesis. Zaragoza, Universidad de Zaragoza, 525pp.

Plunkett, J.M., 1997. Early Diagenesis of Shallow Platform Carbonates in the Oxfordian of the Swiss Jura Mountains. PhD Thesis. Fribourg, Université de Fribourg, unpublished, 166pp.

Riboulleau, A., Baudin, F., Daux, V., Hantzpergue, P., Renard, M., Zakharov, V., 1998. Evolution de la paléotempératures des eaux de la plateforme russe au cours du Jurassique supérieur. Comptes Rendus de l'Académie des Sciences de Paris, Sciences de la Terre et des Planètes, 326, 239-246.

Richter, D.K., Götte, T., Götze, J., Neuser, R.D., 2003. Progress in application of cathodoluminescence (CL) in sedimentary geology. Mineral Petrology, 79(3-4), 127-166.

Rosales, I., Quesada., S., Robles, S., 2001. Primary and diagenetic isotopic signals in fossils and hemipelagic carbonates: the Lower Jurassic of northern Spain. Sedimentology, 48, 1149-1169.

Salas, R., Guimerà, J., 1996. Rasgos estructurales principales de la cuenca cretácica inferior del Maestrazgo (Cordillera Ibérica oriental). Geogaceta, 20(7), 1704-1706.

Savard, M.M., Veizer, J., Hinton, R.H., 1995. Cathodoluminescence at low Fe and Mn concentrations: A SIMS study of zones in natural calcites. Journal of Sedimentary Research, 65(1a), 208-213.

Schobben, M., Ullmann, C.V., Leda, L., Korn, D., Struck, U., Reimold, W.U., Ghaderi, A., Algeo, T.J., Korte, C., 2015. Discerning primary versus diagenetic signals in carbonate carbon and oxygen isotope records: An example from the Permian–Triassic boundary of Iran. Chemical Geology, 422, 94-107.

Sequero, C., Bádenas, B., Aurell, M., 2018. Facies mosaic in the inner areas of a shallow carbonate ramp (Upper Jurassic, Higueruelas Fm, NE Spain). Facies, 64(2), 1-23.

Sequero, C., Aurell, M., Bádenas, B., 2019. Sedimentary evolution of a shallow carbonate ramp (Kimmeridgian, NE Spain): Unravelling controlling factors for facies heterogeneities at reservoir scale. Marine and Petroleum Geology, 109, 145-174.

Sequero, C., Aurell, M., Bádenas, B., 2020. Oncoid distribution in the shallow domains of a Kimmeridgian carbonate ramp (Late Jurassic, NE Spain). Sedimentary Geology, 398, 105585.

Sharp, Z., 2007. Principles of stable isotope geochemistry. Pearson/Prentice Hall, University of Michigan, 344pp.

Soria, A.R., Martín-Closas, C., Meléndez, A., Meléndez, N., Aurell, M., 1995. Estratigrafía del Cretácico inferior del sector central de la Cordillera Ibérica. Estudios Geológicos, 51, 141-152.

Strasser, A., 2015. Hiatuses and condensation: an estimation of time lost on a shallow carbonate platform. The Depositional Record, 1(2), 91-117.

Swart, P.K., 2015. The geochemistry of carbonate diagenesis: the past, present and future. Sedimentology, 62(5), 1233-1304.

Swart, P.K., Oehlert, A.M., 2018. Revised interpretations of stable C and O patterns in carbonate rocks resulting from meteoric diagenesis. Sedimentary Geology, 364, 14-23.

Travé, A., Nadal, J., Playà, E., Salas, R., Martín-Martín, J.D., Gomez-Rivas, E., 2019. Fracture-related dolomitization affecting Late Jurassic-Lowermost Cretaceous syn-rift deposits (Maestrat Basin, Southern Iberian Chain, Eastern Spain). In: Doronzo, D.M.., Schingaro, E., Amstrong-Altrin, J.S., Zoheir, B. (eds.). Petrogenesis and Exploration of the Earth's Interior. Advances in Science, Technology and Innovation, 163-165.

Tucker, M.E., 1993. Carbonate diagenesis and sequence stratigraphy. Sedimentology Reviews, 1, 51-72.

Veizer, J., Bruckschen, P., Pawellek, F., Diener, A., Podlaha, O.G., Carden, G.A.F., Jasper, T., Korte, C., Strauss, H., Azmy, K., Ala, D., 1997. Oxygen isotope evolution of Phanerozoic seawater. Palaeogeography, Palaeoclimatology, Palaeoecology, 132, 159-172.

Vincent, B., Emmanuel, L., Loreau, J.P., 2004. Significance of the isotopic signal ($\delta^{18}O$, $\delta^{13}C$) of neritic carbonates: diagenetic component and original component (Upper Jurassic of the East of the Paris Basin, France). Comptes Rendus Geoscience, 336(1), 29-39.

Vogel, J.C., 1993. Variability of carbon isotope fractionation during photosynthesis. In: Ehleringer, J.R., Hall, A.E., Farquhar, G.D. (eds.). Stable Isotopes and Plant Carbon–Water Relations. San Diego (California), Academic Press, 29-38.

Wierzbowski, H., 2004. Carbon and oxygen isotope composition of Oxfordian–Early Kimmeridgian belemnite rostra: palaeoenvironmental implications for Late Jurassic seas. Palaeogeography, Palaeoclimatology, Palaeoecology, 203, 153-168.

Zuo, F., Heimhofer, U., Huck, S., Bodin, S., Erbacher, J., Bai, H., 2018. Coupled $\delta^{13}C$ and $^{87}Sr/^{86}Sr$ chemostratigraphy of Kimmeridgian shoal-water deposits: A new composite record from the Lower Saxony Basin, Germany. Sedimentary Geology, 376, 18-31.

Manuscript received March 2021;
revision accepted November 2021;
published Online November 2021.